

THREE-DIMENSIONAL IDENTIFICATION AND RECONSTRUCTION OF GALAXY SYSTEMS WITHIN DEEP REDSHIFT SURVEYS

CHRISTIAN MARINONI, MARC DAVIS, JEFFREY A. NEWMAN, AND ALISON L. COIL
 Department of Astronomy, University of California at Berkeley, Berkeley, CA 94720-3411, US
 e-mail: marinoni@astro.berkeley.edu, marc@astro.berkeley.edu, jnewman@astro.berkeley.edu,
 acoil@astro.berkeley.edu
ApJ, submitted

ABSTRACT

We have developed a new geometrical method for identifying and reconstructing a homogeneous and highly complete set of galaxy groups in the next generation of deep, flux-limited redshift surveys. Our method combines information from the three-dimensional Voronoi diagram and its dual, the Delaunay triangulation, to obtain group and cluster catalogs that are remarkably robust over wide ranges in redshift and degree of density enhancement. As free byproducts, this Voronoi-Delaunay method (VDM) provides a non-parametric measurement of the galaxy density around each object observed and a quantitative measure of the distribution of cosmological voids in the survey volume. In this paper, we describe the VDM algorithm in detail and test its effectiveness using a family of mock catalogs that simulate the DEEP2 Redshift Survey. We show that this survey will be quite suitable for optically selecting distant clusters at $z \sim 1$ over a wide range of richness.

Using the mock DEEP2 catalogs, we demonstrate that the VDM algorithm can be used to identify a homogeneous set of groups in a magnitude-limited sample ($I_{AB} \leq 23.5$) throughout the survey redshift window $0.7 < z < 1.2$. The actual group membership can be effectively reconstructed even in the distorted redshift space environment for systems with line of sight velocity dispersion σ_{los} greater than $\approx 200 \text{ km s}^{-1}$. By applying the sampling rate and the instrument-imposed target selection biases expected for DEEP2, we show that we can construct a homogeneous sample of systems which reproduces major properties of the “real” cluster parent population down to $\approx 200 \text{ km s}^{-1}$ for systems with at least 5 members. In a Λ CDM cosmology this translates into an identification rate of ~ 270 systems per square degree and a total of more than 1000 groups within the full DEEP2 survey volume.

By comparing the galaxy cluster catalog derived from the mock DEEP2 observations to the underlying distribution of clusters found in real space with much fainter galaxies included (which should more closely trace mass in the cluster), we can assess completeness in velocity dispersion directly. We conclude that the recovered DEEP2 group and cluster sample should be statistically complete for $\sigma_{los} \gtrsim 400 \text{ km s}^{-1}$. Finally, we argue that the reconstructed bivariate distribution of systems as a function of redshift and velocity dispersion reproduces with high fidelity the underlying real space distribution and can thus be used robustly to constrain cosmological parameters.

Subject headings: galaxies: high-redshift – galaxies: clusters: general – cosmology: large-scale structure of the universe – methods: data analysis

1. INTRODUCTION

Non-linear galaxy overdensities provide useful cosmological probes, particularly as objects ranging from small groups to rich clusters can be described simultaneously using relatively simple empirical and theoretical distributions. Marinoni & Hudson (2001), for example, were able to investigate the mapping between mass, light, and other cluster observables for objects ranging from $\sim 10^{12}$ to $\sim 10^{15} M_{\odot}$ in mass. The abundance of groups and clusters itself is a fundamental observable expected to have evolved substantially since high redshift, with the strength of that evolution sensitively dependent upon fundamental cosmological parameters (Lilje 1992; Bahcall et al. 1997). Newman et al. (2001) have shown that this variant of the classical dN/dz test can provide significant constraints on “dark energy” models when applied to upcoming redshift surveys. However, a key issue in whether we can use clusters to make precision cosmological measurements is the availability of efficient and objective cluster-finding algorithms.

In recent years there has been much work on detecting two-dimensional galaxy overdensities in wide-field optical imaging surveys for subsequent spectroscopic follow up (Scodeggio et al. 1999; Gal et al. 2000; Gladders & Yee 2000; Gonzales et al. 2001). However, these systematic searches for clusters, fueled by the availability of large CCD camera mosaics, are in many cases biased towards special subsets of the general galaxy population such as red objects or AGNs. A closely related problem is that the recovered cluster samples are statistically complete only near the upper tail of the velocity dispersion distribution. In effect, these methods identify only those rich aggregates that are most conspicuous. However, less extreme systems such as galaxy groups, which contain most of the luminosity, and presumably mass, of the universe, may be more useful probes of the large-scale structure.

With the next generation of multi-object spectrographs on large telescopes soon to be installed, deep redshift surveys (e.g., the DEEP2/DEIMOS Survey (Davis et al. 2000), hereafter referred to as DEEP2, and the

VLT/VIRMOS redshift survey (Le Fèvre *et al.* 2001)) are well within reach. It is thus worthwhile to address the more ambitious task of constructing large, statistically complete samples of galaxy systems selected over wide redshift baselines and covering a broad range in density enhancement and velocity dispersion using the three-dimensional redshift space data such surveys will provide.

Because of the high spectroscopic resolution (FWHM $\sim 65 \text{ km s}^{-1}$) and relatively dense sampling to be used, the DEEP2 Redshift Survey will be uniquely suitable for measuring the velocity dispersions and the internal dynamics of large numbers of distant galaxy clusters, and selecting a group sample without relying on non-kinematic properties (X-ray brightness, galaxy richness in optical images, etc.). DEEP2 will obtain data characterizing galaxies and large-scale structure that are comparable to those provided by the best previous surveys of the local universe, but for objects at high redshift, $z \sim 1$. Furthermore, sensitive S-Z observations are planned for all DEEP2 fields, which will allow the virialization state of clusters to be assessed.

If we are to use DEEP2 clusters to make cosmological measurements, we must be able to reliably identify high redshift groups and clusters and determine their members and properties robustly. However, rich clusters are rare events; only ~ 10 Coma-like clusters are expected in the DEEP2 survey volume. The mass function of clusters is very steep, so to overcome Poisson noise detecting the most abundant groups of lower mass is critical. To improve the predictive power of the cosmological tests, we must be able to identify systems down to small, group-scale velocity dispersions (σ_{los}) in a complete and unbiased way.

A variety of methods for identifying galaxy overdensities have been applied to redshift surveys of the local, $z \sim 0$ universe. The hierarchical (Materne 1978; Tully 1980) and percolation (also known as “friends-of-friends”, hereafter simply FOF) methods (Huchra & Geller 1982) of group identification have both been widely used (e.g. (Tully 1987; Maia, da Costa & Latham 1989; Ramella, Geller & Huchra 1989; Haynes & Giovanelli 1991; Gourgoulhon, Chamaraux & Fouqué 1992; Nolthenius 1993; Garcia 1993; Ramella, Pisani & Geller 1997; Trasarti-Battistoni 1998; Ramella *et al.* 1999; Giuricin *et al.* 2000; Tucker *et al.* 2000)). Their main characteristics and drawbacks are discussed in Marinoni (2001).

These standard cluster-finding algorithms are unsatisfactory for many reasons. For instance, the fixed-radius search window at the heart of standard FOF techniques is insensitive to local variations in the density of points. Assigned cluster membership therefore depends on the scale of the adopted linking length and not the distribution of galaxies alone, violating the dictum to “let the data speak for themselves” (Openshaw 1984). In fact, both the hierarchical and the percolation methods require prior knowledge and/or user-fixed parameters to produce their best results. Density thresholds, linking length parameter scaling laws, galaxy selection functions, etc. must all be set in advance. The pre-processing and/or trial-and-error tests required to tune these algorithms for a particular dataset is extremely inefficient and may even lead to systematic

differences amongst different applications of the same technique.

It is well known that the performance of the standard FOF algorithm across a wide range of density enhancements is not uniform (Frederic 1995a,b). A generous linking length is preferred in studies which aim to identify high-velocity dispersion systems. On the other hand, studies of loose associations require short velocity links, but this can result in a bias towards low velocity dispersion measurements. In general, the velocity dispersion of systems identified with the FOF algorithm is $\sim 30\%$ higher than the velocity dispersion of groups identified in the same galaxy catalog by the hierarchical method (Garcia 1993; Giuricin *et al.* 2001). To further complicate matters, clusters identified with one method may not be detected by the other.

Given the failings of traditional three-dimensional cluster identification methods, which are likely to only be worse at high redshift (due to evolutionary effects, sparse sampling etc.), we have attempted to develop a new algorithm that may be applied to future redshift surveys such as DEEP2. This paper presents a new technique for finding systems of galaxies from redshift space maps, designed with the goal of matching their underlying, real space distribution. Our algorithms for cluster detection and reconstruction use three-dimensional Voronoi-Delaunay methods (hereafter VDM) to process the spatial distribution of galaxies, which possess a number of advantages over previous techniques. We also present the results of tests of these techniques using mock catalogs derived from N-body simulations that mirror the properties of the DEEP2 survey. Applying our reconstruction scheme to artificial surveys, where the cluster characteristics are known *a priori* in real space, allows us to clarify the uncertainties and assess the overall performance of the method while at the same time testing the completeness of the resulting catalog of systems.

The Voronoi partition of a space into minimally sized convex polytopes – the three-dimensional analogue of Dirichlet tessellation or determination of Thiessen polygons (Dirichlet 1850; Voronoi 1908) – provides a natural way to find cluster centers (peaks in the galaxy density field) without requiring any arbitrarily chosen window profiles or smoothing length parameters. The Delaunay complex (Delaunay 1934), the simultaneously-determined dual of the Voronoi diagram, implicitly contains vast amounts of proximity information and yields a natural measurement of inter-galaxy scale lengths but is linearly proportional in size to the dataset. The Voronoi-Delaunay structures are a fundamental tool of computational geometry and arise naturally and independently in many different fields (see Aurenhammer (1991) for a very inclusive survey of Voronoi techniques in mathematics and the natural sciences).¹ More recently, the Voronoi diagram has been applied in cosmological contexts to investigate the problem of galaxy formation (e.g., (Matsuda & Shima 1984; Icke, & van der Weigaert 1987; Ling 1987; Yoshioka & Ikeuchi 1989; van der Weigaert & Icke 1989; Coles 1991; Ikeuchi &

¹ In fact, what became known as the Voronoi diagram was first suggested in an astronomical context for a problem similar to that investigated here. In his treatment of cosmic fragmentation *Le monde, ou Le Traité de la Lumière*, posthumously published in 1664, René Descartes used Voronoi-like methods to model the spatial distribution and the relative influence of solar system bodies (see Fig. 7 in Okabe, Boots & Sugihara (1992)).

Turner 1991)). Voronoi-based methods for selecting high-density regions in two-dimensional images have also been developed (e.g., (Ebeling & Wiedenmann 1993; Pasztor 1994; Ramella et al. 2001; Kim et al. 2001)).

Our cluster-finding technique is the logical extension of such methods to the three-dimensional problem of finding clusters in a redshift survey. This VDM algorithm is intended to avoid some of the difficulties which the standard hierarchical and percolation algorithms present, particularly for large surveys covering a wide redshift range. It is a known fact that some cluster parameters are more sensitive to the cluster definition procedure than others. For instance, Marinoni, Hudson & Giuricin (2001) found that the different global light distribution of systems, identified in the Nearby Optical Galaxy (NOG) sample using different standard grouping methods, are consistent with the hypothesis of being drawn from a common underlying parent distribution. Moreover, Giuricin et al. (2001) show that the major dynamical properties of clusters (mass, virial radius, etc.) are relatively unstable, with values depending on how the clusters and their members were identified using standard clustering algorithms. In this paper, we show that our method is optimized to preserve the information encoded in key cluster distribution functions, such as the number density of clusters as a function of their line of sight velocity dispersion $n(\sigma_{los})$ and redshift $n(\sigma_{los}, z)$, even when σ_{los} is as low as 200 km s^{-1} .

The outline of our paper is as follows: in §2, we summarize the major technical characteristics of the DEEP2 Redshift Survey and describe the mock catalogs used to simulate the survey volume and galaxy fluxes. In §3 we present the group-finding algorithm and its technical implementation; in §4 we examine the performance of this algorithm when it is applied to the mock catalogs. In §5 we apply the DEEP2 target selection bias to the mock catalogs and derive the characteristics and size of the expected DEEP2 optical cluster sample. In §6 we investigate the relation between clusters reconstructed applying the VDM to a flux-limited sample of halo galaxies in redshift space to the underlying matter distribution traced by fainter galaxies. Our results are summarized in §7.

2. THE DEEP2 REDSHIFT SURVEY

Once observations commence in the summer of 2002, the DEEP2 Redshift Survey will be uniquely capable of detecting in three dimensions and resolving the velocity structure of clusters and groups of galaxies at high redshift, $z \sim 1$. A new instrument, the Keck II Deep Imaging Multi-Object Spectrograph (DEIMOS; cf. Cowley et al. (1997)), was designed for this project and will be installed in Hawaii early in 2002. DEIMOS can provide imaging or multi-slit spectroscopy over a field of view that is approximately a rectangle of size $16'$ by $5'$ and over the wavelength range $0.42\text{--}1.1 \mu\text{m}$. By using custom-milled slitmasks, DEIMOS can obtain spectra of $\sim 100\text{--}150$ galaxies at a time. This will allow DEEP2 to observe $\sim 60,000$ galaxies with $0.7 < z < 1.2$ (a depth which corresponds to using the 1200 lines/mm grating and a magnitude limit $I_{AB} < 23.5$) over the 120 nights allocated to the project, in addition to a deeper, smaller subsample. The survey should be completed in late 2004. All objects will be ob-

served with much higher spectral resolution than planned for other comparable projects, $R \equiv \lambda/\Delta\lambda \sim 5000$. This resolution will allow DEEP2 to measure redshifts of galaxies to a precision of $< 10 \text{ km s}^{-1}$, readily resolving even small groups.

DEEP2 will target four fields each 2° by 0.5° , which corresponds to comoving dimensions of 80 by $20 h^{-2} \text{ Mpc}^2$ at $z \sim 1$ for a ΛCDM universe. The corresponding line of sight comoving distance from $z = 0.7\text{--}1.2$ is $\sim 1400 h^{-1} \text{ Mpc}$, though as DEEP2 is flux-limited sampling will be sparser at the highest redshifts. The four fields were chosen in low-extinction regions which are continuously observable from Hawaii over a six month interval. One field includes the extended Groth Survey strip (Groth et al. 1994), and two fields are on the equatorial strip which will be deeply imaged by the Sloan Digital Sky Survey (SDSS). Deep *BRI* imaging has been obtained throughout each field using the CFHT 12k camera by Kaiser & Luppino (see Wilson et al. (2000) for details), allowing photometric selection of objects with $z > 0.7$ for spectroscopy. Many observations in other wavebands, including sensitive Sunyaev-Zel'dovich studies in each field, have also been planned.

Because spectra from adjoining slitlets on the same mask cannot be allowed to overlap, slitmask spectroscopy is inevitably unable to target every object in the densest regions. On average, spectra will be obtained for $\sim 70\%$ of all galaxies meeting the DEEP2 selection criteria in each field, but sampling will be lower where galaxies are most densely packed on the sky. Coil, Davis, & Szapudi (2001, hereafter CDS) tested the degree to which this selection bias may affect measurements of the underlying two-point and three-point correlation functions. For that purpose, they created mock catalogs which emulate the properties of a flux-limited DEEP2 sample; we have made use of those same catalogs to test the performance and robustness of our cluster-finding algorithm.

These mock data were constructed from simulations that combined the results of high-resolution, large-volume N-body calculations with semi-analytic methods that model the formation and evolution of individual objects Kauffmann et al. (1999). In particular, the catalogs provided by Kauffmann et al. were based upon the GIF N-body simulations²; CDS used the ΛCDM catalogs, based on a model with $\Omega_{matter}=0.3$, $\Omega_{\Lambda}=0.7$, $h=0.7$, and $\sigma_8=0.9$. To match the DEEP2 survey, CDS then constructed from the Kauffmann et al. results six nearly-independent volumes with the geometry of a DEEP2 field, each covering the equivalent of 2° by 0.5° on the sky and a redshift range of $0.7 < z < 1.2$. At this point, volume-limited samples could be assembled; however, DEEP2 will be a flux-limited survey. Coil, Davis, & Szapudi thus used the absolute magnitudes for each galaxy provided by the semi-analytic calculations to select all objects brighter than the DEEP2 magnitude limit, resulting in six mock catalogs containing $\sim 15,000$ galaxies each. The robustness of the VDM is tested using all six DEEP2 mock catalogs.

3. CLUSTER FINDING METHOD

It is difficult to develop a single method that can robustly identify and determine the membership of groups

² <http://www.mpa-garching.mpg.de/Virgo>

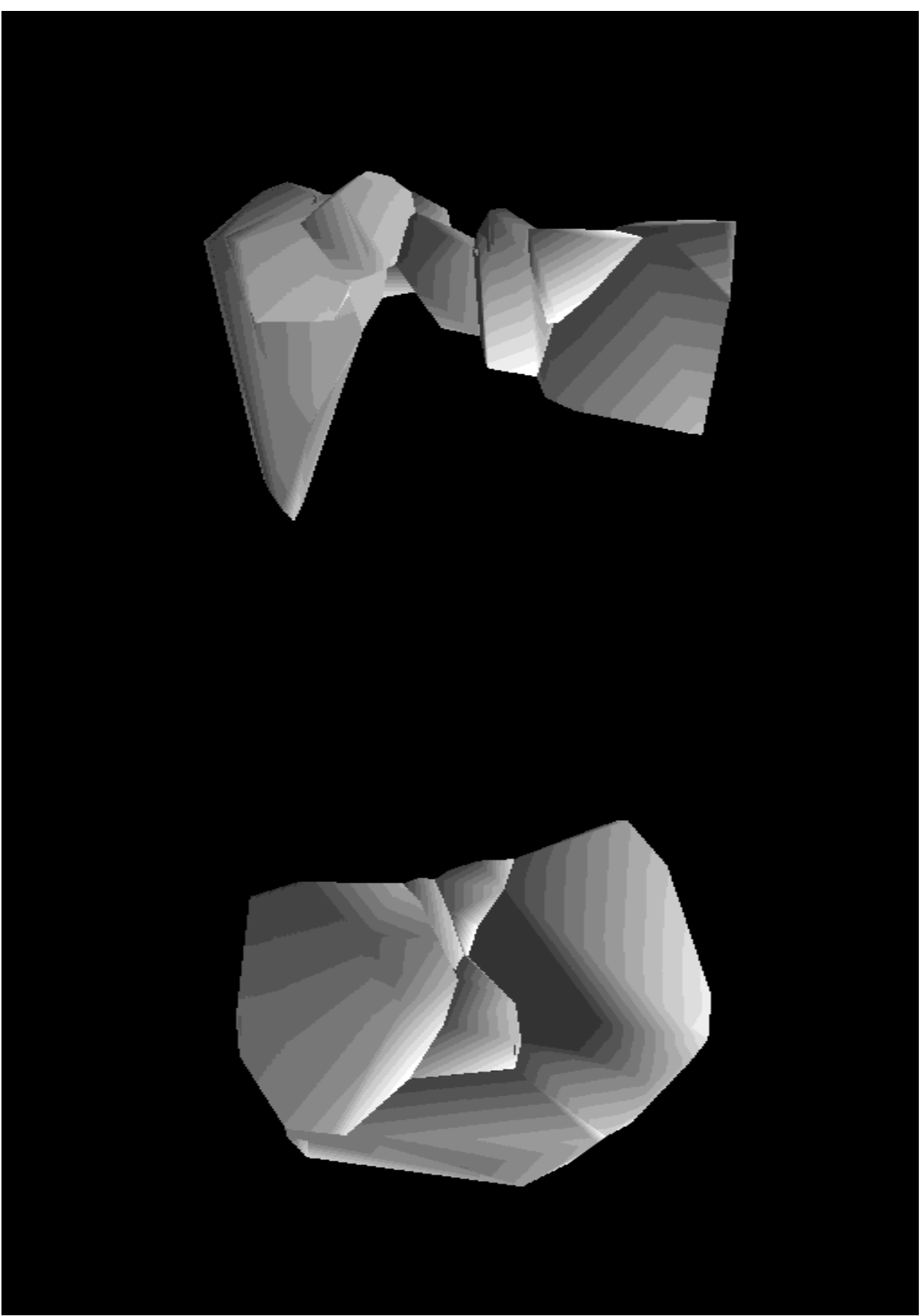


FIG. 1.— Three-dimensional Voronoi reconstruction of a cluster with 10 galaxies in the DEEP2 mock catalog. The Voronoi cells encompassing each cluster galaxy are shown in real space (*bottom*) and in redshift space (*top*). Each Voronoi 3D cell surrounding a galaxy is defined as the intersection of the planes which are perpendicular bisectors of the lines joining that galaxy to the others. Note how the isotropic real-space distribution of cluster galaxies degenerates into a composite Voronoi structure which is elongated along the observer's line of sight.

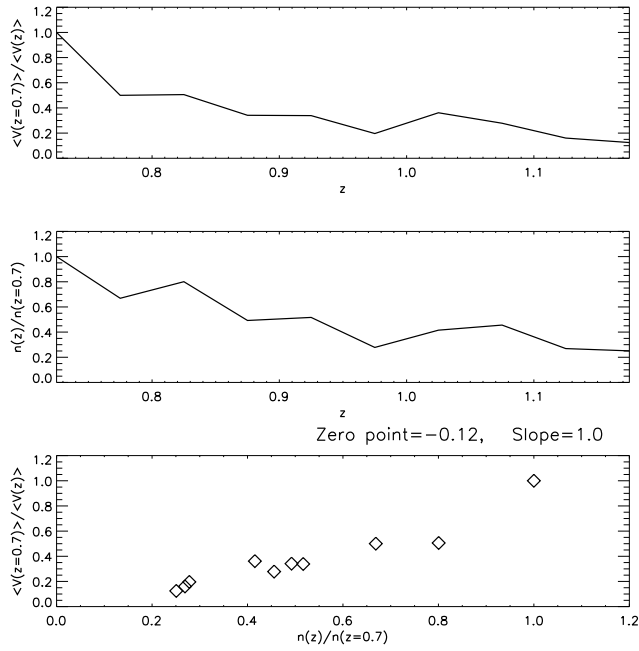


FIG. 2.— The mean galaxy density evaluated by averaging over Voronoi 3D cells contained in a volume $\Delta V (dz=0.05)$ (upper), and by averaging over the counts of galaxies (corrected for relativistic effects) in the same region ΔV (center). Lower: a comparison between the two estimates shows the consistency.

and clusters of galaxies across a wide range of masses and redshifts. These structures may range from $\sim 10^{12} M_\odot$ to $\sim 10^{15} M_\odot$ in mass (with B luminosity varying from $\sim 10^{10} L_\odot$ to $\sim 10^{13} L_\odot$). Moreover, since the mass density of a cluster should depend primarily on its formation time (in the spherical-collapse paradigm), some small groups and rich clusters may have the same mean separation between member galaxies. As a further complication, flux-limited surveys cannot have uniform sampling at all distances. As a result, two groups that have the same physical characteristics (mass, size, richness, etc.) may have different populations of galaxies observed if they are at different redshifts, even without galaxy evolution effects.

We have attempted to overcome these problems, at least in a statistical sense, by taking a computational approach that utilizes both density and spatial proximity information to identify clusters and their members. The Voronoi diagram and Delaunay complex form the basis for this technique. The Voronoi partition provides a geometrically-defined measure of the local density field of a point process, while the Delaunay triangulation contains information on the spatial relationships between those points. We will show that using these tools, we may objectively find clusters and that their intrinsic properties can be reliably measured.

3.1. The Voronoi diagram and Delaunay complex

A Voronoi polyhedron is the uniquely defined convex region of space around a chosen object (also referred to as the “seed”) within which each point is closer to the seed than to any other object. The faces of the Voronoi

cell are formed by planes perpendicular to the vectors between the seed and its neighbors (see figures 1 and 3). The Voronoi partition of a space into minimally sized convex polytopes provides a natural way to measure packing. The volume inside each polyhedron is inversely proportional to the packing efficiency of its seed; a large cell volume indicates that its seed is comparatively isolated.

By performing a Voronoi decomposition on a redshift catalog, we may estimate the three-dimensional galaxy density field in a non-parametric way. Other methods estimate this field by smoothing the distribution of data points with an *a priori* physical model, window profile or binning strategy (Ebeling & Wiedenmann 1993; Marinoni, Hudson & Giuricin 2001). In contrast, the Voronoi diagram provides a density estimator that is asymptotically local (Fadda, Slezak & Bijaoui 1997); the density measured at a position \mathbf{x} is determined completely by the positions of the neighboring data points, while the influence of distant points vanishes.

The Delaunay complex in three-dimensional space is defined by the tetrahedra whose vertices are sets of four galaxies with the property that the uniquely determined sphere circumscribing them does not contain any other galaxy. The center of this sphere is the vertex of a Voronoi polyhedron. The Delaunay triangulation represents the geometrical dual of the Voronoi partition and provides a natural linking structure for a set of objects. A complete treatment of the main mathematical characteristics of these geometrical structures can be found in Zaninetti (1990) or van der Weigaert (1994).

We calculate the Voronoi and Delaunay structures as described in Barber, Dobkin & Huhdanpaa (1996) and compute moments over each Voronoi cell (volume, center of mass, and moment of inertia) following the prescriptions of Mirtich (1996) to transform volume integrals within a polyhedron into explicit sums over its vertices. As an example, in figure 2 we show that the mean density obtained by averaging over the ensemble of Voronoi cells, $\langle 1/V_i \rangle_V$, agrees with the standard density estimator N/V , where N is the total number of objects and V is the volume over which the average is computed.

3.2. Details of the algorithm

Once the Voronoi/Delaunay calculation for a catalog of galaxies in the Doppler distorted redshift space (we know real positions and peculiar velocities for each galaxy in the catalog) has been completed, our algorithm proceeds in three phases. First, global minima of the Voronoi cell volume (i.e., peaks in the density) are identified and provide candidate locations for cluster centers. The Delaunay mesh then allows us to identify central members of each candidate group and estimate physical properties such as the cluster central density. Finally, these estimates are used to define redshift space windows within which we find each group’s members. In this last step it is the predicted structure of the clusters, inferred from an initial level of grouping, that influences *local* decisions regarding galaxy membership.

Before discussing each step in more detail, we state first the working definition of a cluster we have used to judge the performance of our grouping method.

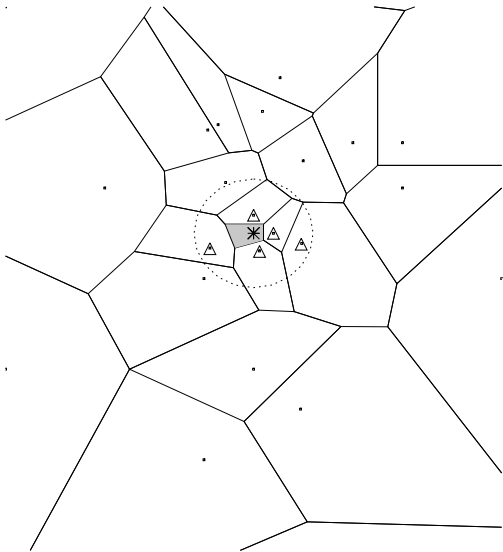


FIG. 3.— Simplified 2-dimensional graphic representation of phase I (§3.2.1). Sky angular coordinates are along the x axis, and the survey depth is displayed along the y axis. Dots represent the galaxy distribution, while the shaded area represents the Voronoi cell surrounding a possible cluster seed (represented by an asterisk). The set formed by the asterisk and the points marked with triangles represents the *first order Delaunay neighbors*.

We consider a cluster to be a system identified as a single group in the real-space, volume-limited DEEP2 mock catalogs using a FOF algorithm with a linking length parameter $b = 0.2$. This parameter value has been shown to effectively select virialized overdensities (mean overdensity ~ 180 in a critical universe), at least in the statistical sense (Cole & Lacey 1996), and it is widely used by simulators in deriving the mass statistics for their N-body halos (e.g. Benson et al. (2000) or Jenkins et al. (2000)); this choice, therefore, facilitates comparison to the literature.

Although this serves to define the set of clusters and their membership in each mock catalog, it is not always desirable to compare a given set of VDM results to this “reality.” For instance, to assess the performance of our method, i.e. determining what fraction of group members are recovered in the same VDM group, we must compare not to the original group membership, but rather only to those members of the actual group which are brighter than the DEEP2 flux limit, as they alone are present in the catalogs to which we apply our algorithm. Except where otherwise specified (e.g. §6), in the remainder of this paper we compare VDM results to the real-space friends-of-friends catalog *after* flux selection; e.g., in §4 we compare the velocity dispersion determined for each VDM cluster to the dispersion calculated from those members of that cluster’s counterpart identified in real space that are brighter than the DEEP2 magnitude limit. Any biases in the DEEP2 VDM sample should then similarly affect the comparison sample, and we can test how well our algorithm reconstructs the information present in the redshift catalog.

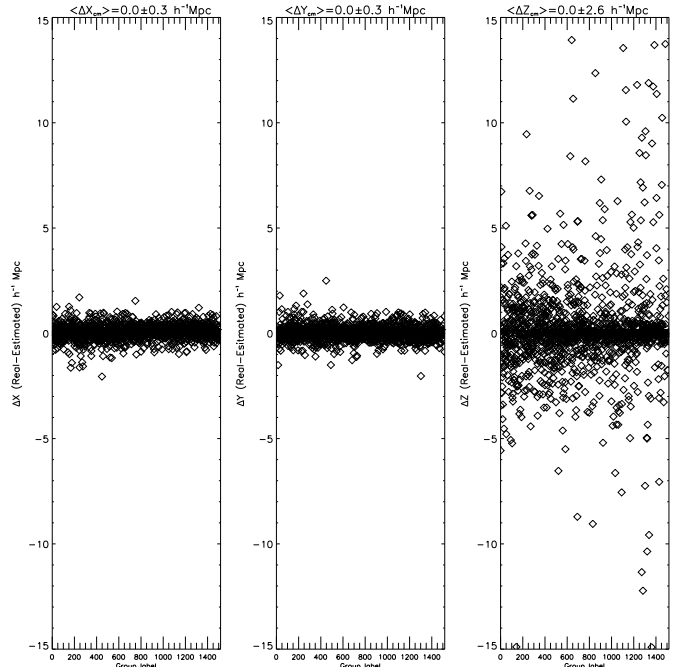


FIG. 4.— Deviations between the three Cartesian components of the estimated group barycenter positions (from the *first-order Delaunay neighbors*) and the center of mass position of the underlying real group. The underlying real structure is computed by determining which members contributing to N_{II} belong to the same structure in real space and using as a reference the biggest of these real systems. Groups are labeled in order of increasing richness along the x axis. On the top of the panel the mean and the 1σ deviations are reported.

3.2.1. Phase I: Finding systems of galaxies

We begin by assuming that the centers of clusters will lie near peaks in the galaxy density field (this assumption is tested below). To identify these peaks, we sort all the galaxies in the catalog by the inverse volume of their Voronoi cell; the smallest cells are most likely to fall at density maxima and are thus potential “seeds” for finding groups or clusters. We must next determine if a given seed actually lies at the heart of a system of galaxies.

Each cluster seed will be linked to its nearest neighbors by the Delaunay mesh. We are interested only in real, physical groupings of galaxies; we therefore must define some *ad hoc* threshold in an attempt to distinguish galaxies that could be physically bound together from galaxies which are in chance proximity to each other. We consider to be neighbors those Delaunay-connected points whose distance from the seed galaxy is less than a fixed limit \mathcal{R}_{\min} . These galaxies, and the original seed galaxy itself, will be referred to hereafter as *first-order Delaunay neighbors* and are used to determine the system’s center of mass.

For this paper we take $\mathcal{R}_{\min} = 1 h^{-1} \text{ Mpc}$ co-moving as standard. In a survey such as DEEP2 that selects galaxies down to $\sim L^*$, a typical loose system like the Local Group would be detected with only 2 elements $\sim 1 h^{-1} \text{ Mpc}$ apart.

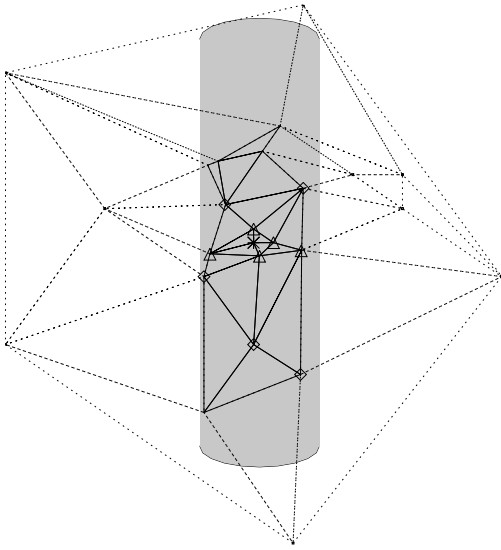


FIG. 5.— Simplified 2-dimensional graphic representation of phase II (§3.2.2). Sky angular coordinates are along the x axis, and the survey depth is displayed along the y axis. Segments represent the Delaunay mesh connecting the galaxy distribution of figure 3. *Second-order Delaunay neighbors* are represented by diamonds. Note that not all the galaxies inside the search window (shaded area) are used to define the projected central density parameter N_{II} , but only those designated by symbols.

This is also the typical mean projected separation between pairs of galaxies within clusters found via a FOF algorithm (Marinoni 2001), and it is the typical central radius of massive clusters as used in studies of the correlation between central richness and velocity dispersions (Bahcall 1981).

If no galaxies satisfy this criterion then the cluster seed will be rejected and considered an isolated galaxy. If, when analyzing a seed we find that all its *first-order Delaunay neighbors* have already been assigned to another structure, we automatically merge the seed galaxy into that system. A schematic representation of this first step in cluster identification is presented in figure 3.

The search radius \mathcal{R}_{\min} , which determines if a point must be considered isolated or not, primarily serves as a parameter controlling the final number of identified systems. The dependence of the cluster statistics on this parameter will be investigated in §4. In this first phase, the search radius allows us to exclude the most deviant points from our center of mass estimates.

Adjusting \mathcal{R}_{\min} within a range $\pm 50\%$ has minimal effects on the derived cluster center positions. In fig. 4 we compare the cluster center of mass recovered in redshift space with the center of mass of the counterpart structure identified in real space. All three spatial components, when averaged over the whole set of mock catalogs, show an offset of zero and a standard deviation less than $0.3 h^{-1}$ Mpc and $2.5 h^{-1}$ Mpc in projection and along the line of sight respectively, testifying to the effectiveness of this technique.

3.2.2. Phase II: Determining clustering strength

Since they are calculated in a parameter-free fashion, both the Voronoi diagram and Delaunay complex are determined isotropically in the angular and redshift directions. However, the peculiar velocities induced by a cluster's gravitational field cause the distribution of galaxies to appear elongated in the redshift direction to a degree determined by its velocity dispersion. The three-dimensional information lost in the transformation to redshift space cannot be recovered uniquely via isotropic, geometric methods; additional assumptions are required to minimize contamination by spurious members. To determine the properties of clusters with any accuracy, we require methods that include this anisotropy.

We therefore define a cylindrical window in redshift space (centered on the barycenter determined in Phase I and circular in the angular dimensions) within which we may find objects which are very likely to be members of each cluster. This cylinder will have radius $\mathcal{R}_{II} \geq \mathcal{R}_{\min}$ and length (along the redshift direction) \mathcal{L}_{II} . We define those galaxies which fall within this cylinder and are connected to first-order Delaunay neighbors by the Delaunay mesh as *second-order Delaunay neighbors*; see figure 5 for a graphical illustration. Note that not all the galaxies in the cylinder are included.

We set $\mathcal{R}_{II} = \mathcal{R}_{\min} = 1 h^{-1}$ Mpc comoving, which is the typical central radius of massive clusters as used in studies of the correlation between central richness and velocity dispersions (Bahcall 1981). Analogous physical considerations guide us to set the half-length of the cylindrical window, \mathcal{L}_{II} , to be $20 h^{-1}$ Mpc. This value includes the upper limit of the peculiar velocity of galaxies that are members of real systems in our simulations (as high as ~ 2000 km s $^{-1}$; cf. 6), taking into account the relativistic stretch factor of ~ 2 in peculiar velocities at redshift $z \sim 1$ (see Appendix A) and the error in the precision with which we can fix the cluster barycenter (see § 3.2.1).

We may use the sum of the numbers of *first- and second-order Delaunay neighbors* as an indicator of the central richness of the group, N_{II} . This parameter ranges from 2 to 25 for the clusters identified in the DEEP2 mock catalogs (note that the cluster seed is included). Since the window has fixed volume, N_{II} corresponds also to an estimate of the central density of galaxies; for less massive systems with small velocity dispersions, it should also be roughly proportional to the projected surface density as measured from images. By including only Delaunay neighbors in N_{II} , we are able to minimize contamination by interlopers, providing a robust estimate even in low-density systems. This is particularly important because N_{II} controls the adaptive window for cluster members used in Phase III.

3.2.3. Phase III: Assigning cluster members

Having detected the center and estimated the richness for each cluster, we then reconstruct the full set of system members. We do this on the basis of physical considerations, not via an empirically tuned parameter threshold. In particular, we exploit the known richness-velocity dispersion correlation to define a search window for each cluster's members based upon its richness.

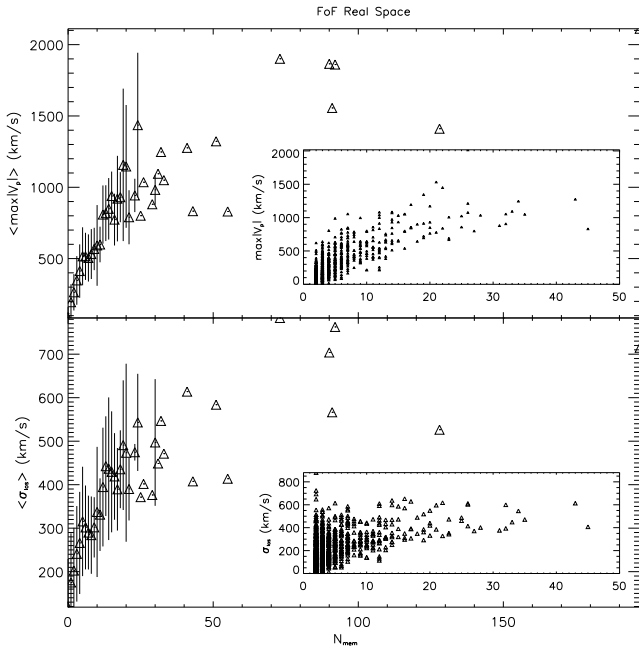


FIG. 6.— *Upper*: the mean of the maximum of the absolute value of the peculiar velocities of real-space identified cluster members, calculated with respect to the cluster barycenter, is shown as a function of the cluster richness (for mock catalog #1). Errorbars represent the 1σ standard deviation of the mean. The inset shows the scatter plot of $\max|v_p|$ as a function of the cluster richness over the lower portion of the richness range. *Lower*: the mean line of sight velocity dispersion is plotted as a function of richness for real-space clusters. The inset shows the scatter plot of the line of sight velocity dispersions as a function of the cluster richness over the lower portion of the richness range.

The virial theorem predicts that velocity dispersion and central number density of galaxies are correlated. Bahcall (1981) observationally confirmed the existence of a strong linear correlation valid from loose groups to clusters. Such a relation in fact holds for the clusters found in our mock catalogs; in figure 7 we show that a linear trend is seen when we plot the maximum peculiar velocity of galaxies in a system (here represented as a distance stretch) versus the cluster central richness. We rely on this relation to estimate the strength of the underlying clustering, which we then use to determine on a group by group basis the window around the system’s center within which to search for Delaunay-connected galaxies.

Specifically, for each cluster we define a cylindrical window (symmetric about the redshift direction) with dimensions determined by the richness scale factor N_{II} and then process the set of Delaunay-connected galaxies inside with a rapidly converging “inclusion-exclusion” logic to identify cluster members within that window. By using the Delaunay mesh to identify the nearby galaxies, we are able to do this quite rapidly; once the initial Voronoi-Delaunay calculation is complete (which need only be done once for a catalog), it takes only 5 minutes on a modern workstation to process ~ 19000 galaxies into a catalog of groups and clusters.

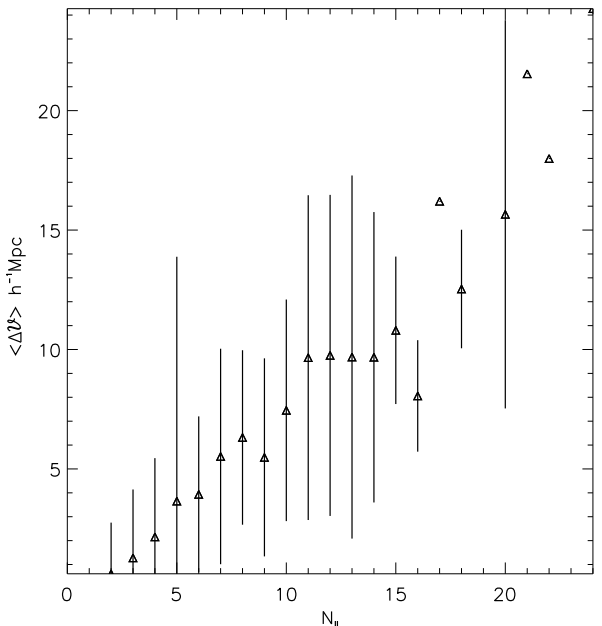


FIG. 7.— Mean line of sight half-length dimensions of real groups as measured in redshift space are plotted versus the central density parameter N_{II} defined in section 3.2.2. The measured elongation is caused by galaxy peculiar velocities.

The radius of the window (in the plane of the sky) and its half-length (in the redshift direction) are determined by the equations:

$$\begin{cases} \mathcal{R} = \max[r \cdot N_{\text{II}}, \mathcal{R}_{\text{II}}] \\ \mathcal{L} = \max[v \cdot N_{\text{II}}, \mathcal{L}_{\text{min}}] \end{cases} \quad (1)$$

where r and v are coefficients that fix the scale of the window in each direction and \mathcal{L}_{min} is a cutoff filter required to take into account the loss of distance resolution on small scales from the smearing caused by peculiar velocities.

We have determined r and v by requiring that when N_{II} takes its maximum possible value, the window has dimensions \mathcal{R}_{max} and \mathcal{L}_{max} that correspond to the maximum radius and peculiar velocity expected for a cluster in a DEEP2 field. Guided by our mock catalogs and literature data (Abell 1958; Bahcall 1988; Borgani et al. 1997) we assume that such a cluster is characterized by $\mathcal{R}_{\text{max}} \sim 1.5 h^{-1} \text{Mpc}$ comoving and $\mathcal{L}_{\text{max}} = \mathcal{L}_{\text{II}} = 20 h^{-1} \text{Mpc}$ (we expect ~ 1 Coma-like cluster with 1000 km s^{-1} dispersion in each DEEP2 field of volume $\gtrsim 10^6 h^{-3} \text{Mpc}^3$). \mathcal{R}_{max} then matches the Abell radius (Abell 1958) while the value of \mathcal{L}_{max} has already been justified in the previous section. In a similar way, the threshold filter $\mathcal{L}_{\text{min}} = 5 h^{-1} \text{Mpc}$ is set by noting that it is common to have at least one member with a peculiar velocity of 500 km s^{-1} with respect to the cluster barycenter, even in systems of very low richness (see figure 6). Although plausible physical considerations have led to our definition of the window size, it may also be justified *a posteriori* by the good agreement of the derived cluster membership with that found by FoF in real space (see §4).

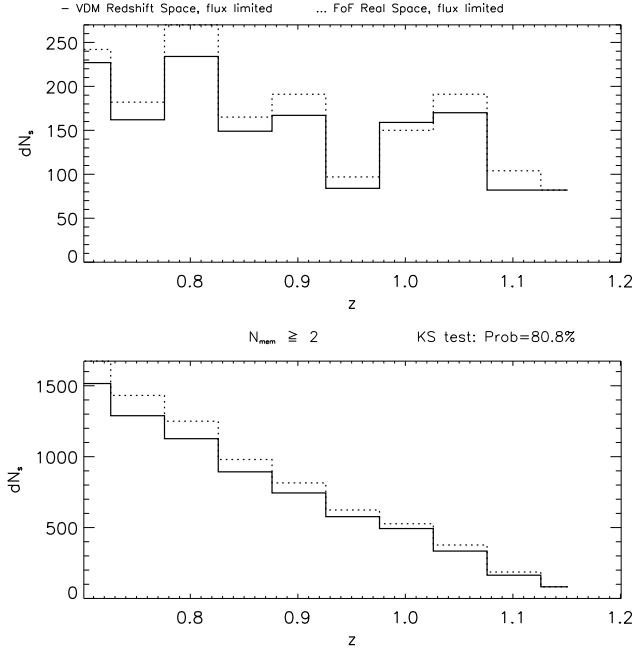


FIG. 8.— Differential (*upper*) and cumulative (*lower*) distributions of clusters identified by VDM in mock #1 (whose galaxy distribution is shown in figure 10 and 11) as a function of redshift. The parent distribution (clusters identified in real space) is the dotted line, while the observed distribution recovered by VDM in redshift space is represented by the solid line. Data are binned in redshift intervals of width 0.05. A Kolmogorov-Smirnov statistical test confirms the consistency and the lack of any identification bias.

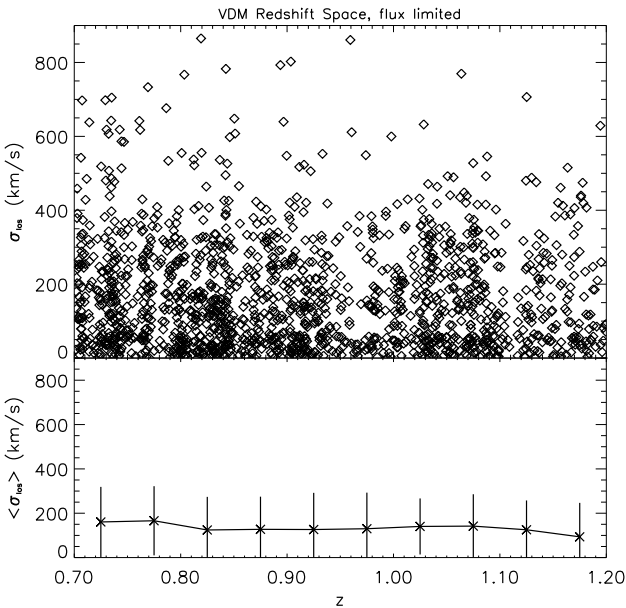


FIG. 9.— *Upper*: velocity dispersions of the reconstructed groups ($N_{\text{mem}} \geq 2$) in the mock #1 catalog are plotted versus the survey depth. *Lower*: the same data averaged in redshift bins of width 0.05. Errorbars represent the standard deviation of the velocity dispersions of all systems in each bin.

Since the size of the search window depends upon the richness estimate of phase II, to ensure a uniform population of clusters we must correct that estimate for the variation of the DEEP2 luminosity limit with redshift. We do this based upon the scaling of the Voronoi cell volume as a function of redshift; as the sampling decreases at greater distance, the density of objects in the sample will become lower and thus the mean volume of the cells larger. We therefore correct a value of N_{II} at redshift z to

$$N_{\text{II,corr}} = N_{\text{II}} \cdot \left(\frac{\langle V(z) \rangle}{\langle V(z=0.7) \rangle} \right)^a, \quad (2)$$

where V is the volume of a Voronoi cell and a is a free parameter we fit by comparing the scaling with distance of the reconstructed number of clusters with the analogous quantity calculated in the volume-limited real space simulation (see figure 8.)

Although one might expect $a = 1/3$ from simple scaling arguments, for the mock DEEP2 catalogs we find a is consistent with being $\lesssim 0.1$; i.e., the sizes of the windows need be only weakly dependent on the galaxy density gradient. There are two reasons for this: first, in the *identification* phase, the Voronoi partition highlights regions of enhanced clustering, where galaxies tend to be more luminous (Park et al. 1994; Giuricin et al. 2001). This can be appreciated in figure 8 where we plot the distribution of the number of identified systems as a function of distance and show the lack of any identification bias. Second, the centrally static logic of our *reconstruction* phase bypasses the problem common to other methods (which usually link successive elements only relative to the last merged unit) of breaking a distant system into sub-units as soon as faint linking elements disappear under the visibility threshold of the survey. This can be inferred in figure 9 where no systematic correlation of the recovered velocity dispersion with survey depth is apparent.

This is reassuring, since in contrast the measured velocity dispersion is known to critically depend on the adopted percolation length in the FOF algorithm (Nolthenius & White 1987), and often shows an unwanted dependence on distance. One reason why our cluster-finding algorithm is more robust than percolation methods in redshift space is that cluster membership is always determined within a limited window around the known cluster center, rather than relative to the last merged unit. This suppresses the non-physical structures sometimes identified by the FOF method, such as apparent long filaments that are often due to two physically unrelated systems linked in redshift space by member galaxies with extreme peculiar velocities.

4. STATISTICAL TESTS OF THE ALGORITHM

Having defined an algorithm, we now test its stability and effectiveness for robustly detecting clusters over a wide range of richness and over a broad redshift baseline. Such a comparison requires great care; the identification of clusters in redshift space and the measurement of their parameters in an unbiased way are inherently difficult, even in the local universe. Since the galaxy correlation function is positive over a wide range of physical scales, cluster definition is inevitably sensitive to the selection window. However, in what follows, we will show that some cluster parameters may be less sensitive to how clusters are identified than others.

We are concerned in this section only with testing our method's potential performance; to this purpose, we use all the galaxies within each mock catalog that satisfy the magnitude and redshift conditions $I_{AB} \leq 23.5$ and $0.7 < z < 1.2$. We defer discussion of the DEEP2 target selection bias, which limits the number of galaxies for which the survey will be able to provide redshift measurements in dense regions, to § 5.

In figure 10 we present a mock catalog for one DEEP2 field collapsed along the smallest axis, covering the redshift range $z=0.7-1.2$ and containing a volume of roughly $10^6 h^{-3}$ Mpc comoving (~ 15000 galaxies). We also show the real-space distribution of members of those FoF groups with $N_{mem} \geq 5$ elements above the survey magnitude limit (central panel) and the reconstructed population of galaxies assigned to systems with at least 5 elements by our Voronoy-Delaunay algorithm operating in redshift space (lower panel). In figure 11 we show the 2-dimensional sky distribution using angular coordinates for the same sample of objects. Using these graphic projections we can qualitatively compare the space distributions of real structures defined above with the space distribution of clusters recovered in the redshift space flux-limited sample by the VDM. Note how in both cases the large scale patterns defined by galaxy systems and the associations of clusters in higher-order structures reproduce the underlying real space landscape.

To assess the performance of our cluster-finding algorithm, we can test the statistical consistency between the distributions of the cluster parameters of interest recovered in redshift space and the corresponding distributions inferred from those members of the clusters identified in real space that are above the survey magnitude limit.

We use several physical properties as indicators to probe the reliability and effectiveness of the VDM: viz., richness, velocity dispersion, mass, and redshift distribution. For instance, figure 12 shows how well we are able to reproduce the actual cumulative distribution function for the richness of clusters in one of our mock catalogs. The same level of accuracy is achieved in each mock catalog. We note that the total number of systems recovered by the VDM when the parameter \mathcal{R}_{min} is varied up to 20% of its assumed value (see §3.2.1) is always within 20% of the real total number of systems. This insures that the VDM, besides the intrinsic scaling, also preserves the absolute normalization of the relation.

A quantitative test of the one-to-one correspondence between reconstructed and real groups can be performed by counting the number of members of each reconstructed cluster that belong to a common real group. We first determine which members of each real group belong to the same reconstructed systems. We may then define the largest group fraction (LGF) for each real group by dividing the number of members in its largest redshift-space subgroup by the total number of members in the real group (see Frederic (1995a) and Giuricin et al. (2000) for a similar definition of the LGF). If a cluster is identified in redshift space as a single system with all of its members, it would have an LGF of 100%, while if none of its members were assigned to groups in common its LGF would approach 0.

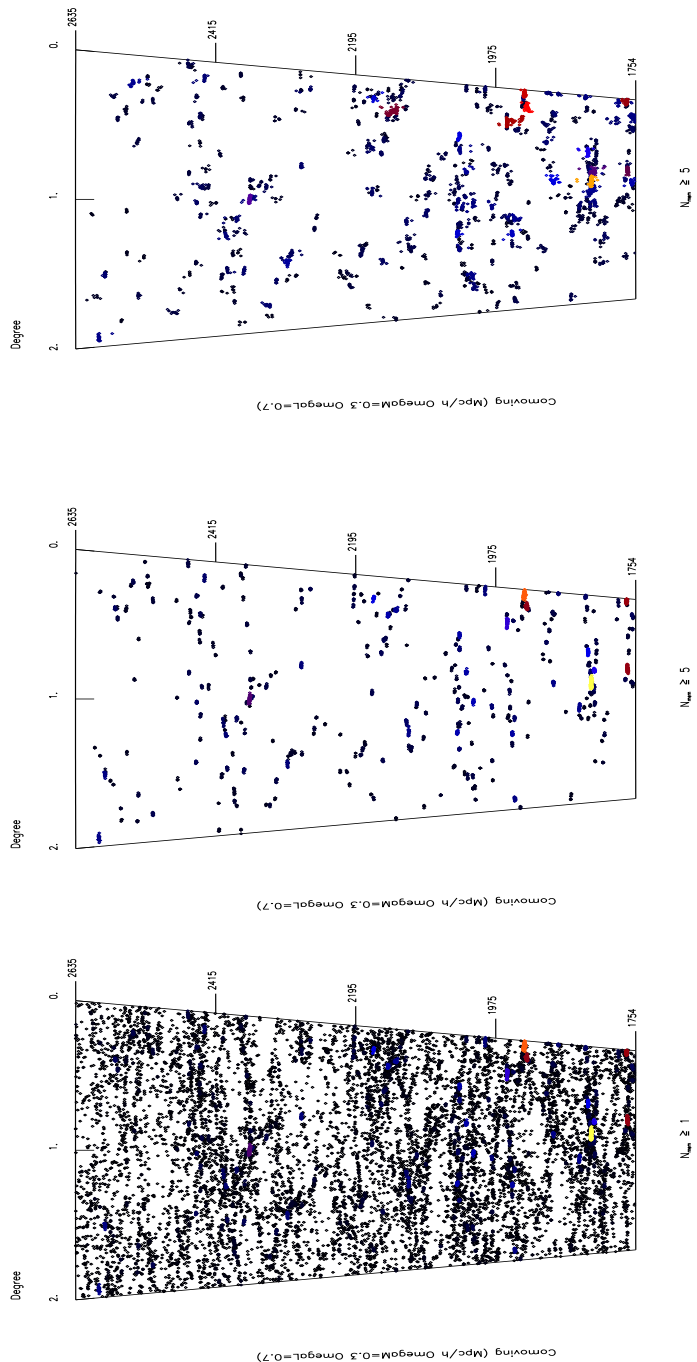


FIG. 10.— *Left*: all galaxies in one of our DEEP2 mock catalogs (#1) represented in a 2D, real-space cone diagram. The surveyed volume corresponds to an angular area of 1 square deg and to the redshift interval $z=0.7-1.2$ (here expressed in h^{-1} Mpc units). *Center*: real space, large-scale spatial distribution of galaxies belonging to clusters with more than 5 members as identified using the FOF algorithm. *Right*: real space, large-scale spatial distribution of galaxies belonging to clusters with more than 5 members as reconstructed by the VDM algorithm in redshift space.

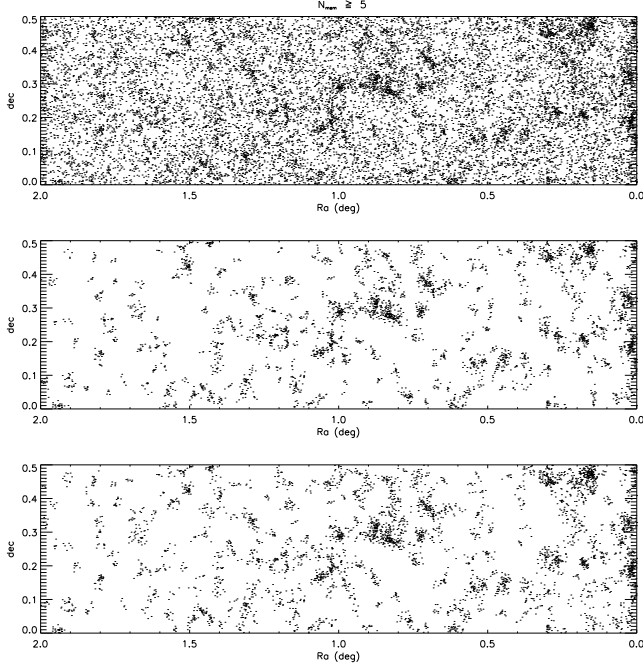


FIG. 11.— *Upper*: sky distribution in angular coordinates of all the galaxies brighter than the DEEP2 limit extracted from mock catalog #1. *Center*: sky distribution of those galaxies belonging to real-space identified groups with $N_{mem} \geq 5$ elements. *Lower*: sky distribution of galaxies associated to groups with at least 5 elements as determined by our VDM algorithm applied in redshift space.

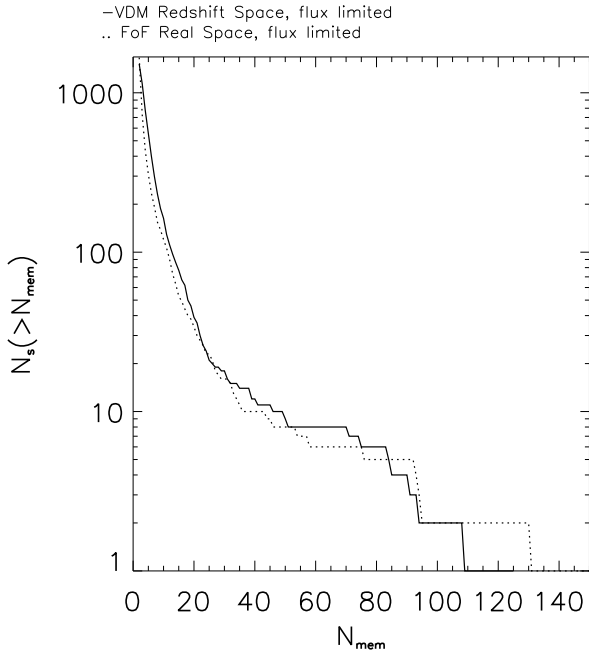


FIG. 12.— Cumulative distribution functions (in logarithmic units) of the real or reconstructed system richness of clusters in mock catalog #1.

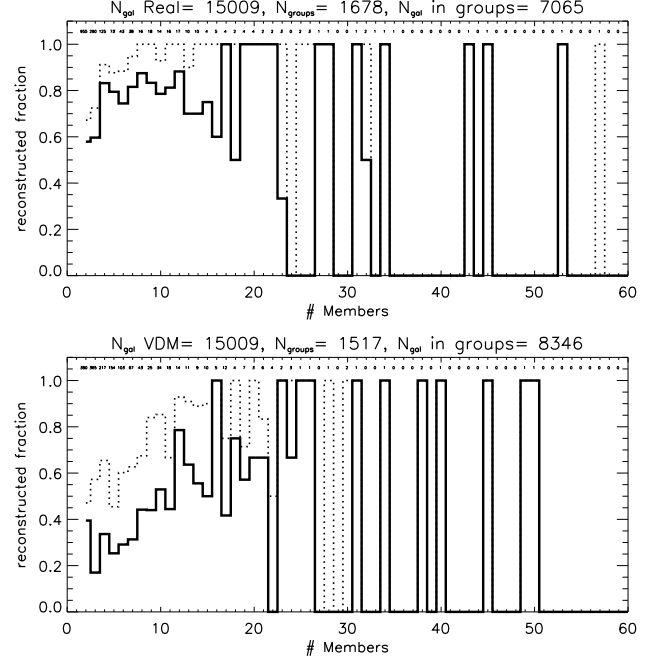


FIG. 13.— *Upper*: histogram of the largest group fraction (LGF; see §4 for definition) as a function of the number of galaxy members in the groups identified in real space. The solid line gives the fraction of redshift-space recovered groups with LGFs between 75% and 100%, while the dotted line corresponds to LGFs greater than 50%. The numbers at the top of each bar is the total number of systems in real space with that given number of members. *Lower*: the largest group fraction as a function of the number of galaxy members in groups identified in redshift space.

The upper panel of figure 13 shows, as a function of group richness (number of members), the fraction of real groups having a given LGF. For example, there are 15 real groups with 10 elements; of these, 70% have 75% - 100% of their elements identified as belonging to the same group in redshift space, while 80% of them have an LGF of at least 50%. The large fraction of groups having high LGF values provides a quantitative example of the effectiveness of our cluster membership determination. Symmetrically, we can define the LGF of systems identified in redshift space using their subgroups found in real space. The histogram of the largest group fraction as a function of the number of galaxy members identified in redshift space is shown in the lower panel of the same figure. Here we can appreciate the contribution of interlopers, which tend to spuriously increase the number of members in the reconstructed group for systems with less than 30 elements. However, again the high fraction of groups with LGF of at least 50% confirms the utility of our strategy.

A useful cluster sample must satisfy well-defined selection criteria, possibly maximizing the number of objects meeting the completeness limits. In many dynamical studies it is imperative to collect a sample of clusters complete with respect to the velocity dispersion parameter (Borgani et al. 1997).

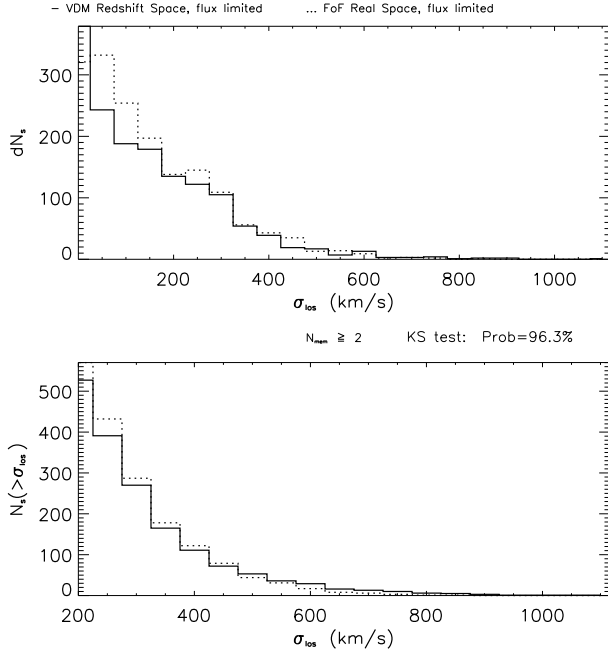


FIG. 14.— Differential (*upper*) and cumulative (*lower*) distributions of the number of clusters with $N_{mem} \geq 2$ detected and reconstructed in mock catalog #1 as a function of their 1D projected velocity dispersions. The distribution of clusters identified by FoF in real space is shown by the dotted line, while the distribution recovered by VDM in redshift space is the solid line. Data are binned in velocity dispersion intervals of width 50 km s^{-1} . A Kolmogorov-Smirnov test confirms the consistency.

However, most workers have selected samples complete to some richness, and assumed that this translates into a completeness in σ_{los} , although it is well known that samples collected in this way are usually biased towards low σ_{los} values (Mazure *et al.* 1996; Biviano *et al.* 1998). As we are most interested in the cluster velocity function, we adopt a different approach here.

In figure 14 we plot both the differential and cumulative distribution of the number of clusters found in one mock DEEP2 field as a function of the projected line of sight velocity dispersion σ_{los} for both the real-space FoF and redshift-space VDM samples. A Kolmogorov-Smirnov statistical analysis (KS) quantifies the level of agreement between the intrinsic cumulative velocity function of the DEEP2 sample and the one recovered in redshift space. The plot shows how the VDM can reliably identify an homogeneous set of systems which reproduce real clusters characteristics down to $\sigma_{los} \approx 200 \text{ km s}^{-1}$. These results must be compared to standard techniques of cluster identification and interloper rejection which are systematically affected by observational biases for $\sigma_{los} \leq 600 \text{ km s}^{-1}$ (Borgani *et al.* 1997).

By analyzing the six different mock catalogs, we find that the average number of real (FoF) clusters with $N_{mem} \geq 2$ members a simulated DEEP2 field is 601 ± 43 , while the average number of systems reconstructed in redshift space by the VDM is 571 ± 46 , with a satisfactory average KS probability value of $(55 \pm 35)\%$. We may check the stability of the final cluster sample properties by varying the clustering parameter \mathcal{R}_{min} .

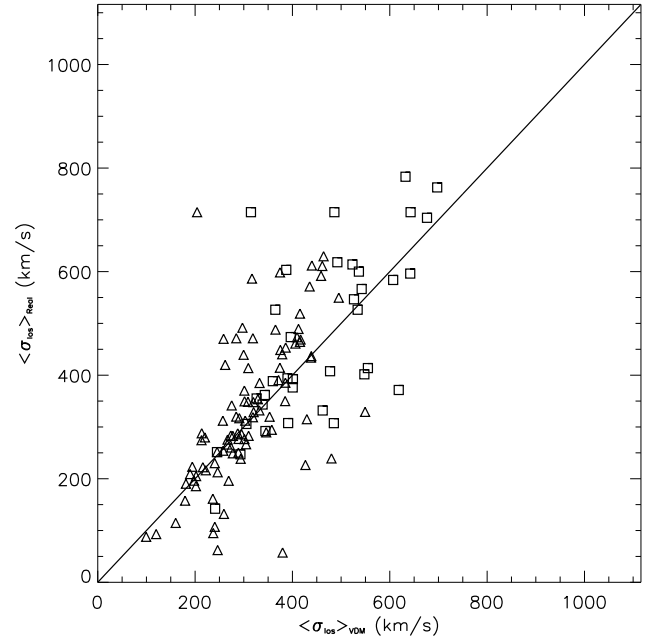


FIG. 15.— Real and recovered velocity dispersions of systems with $N_{mem} \geq 10$ elements are compared. For each recovered system, the corresponding real-space structure is identified by determining which group members belong to the same structure in real space and using as a reference the largest of these real systems. Systems with $10 \leq N \leq 20$ and with $N > 20$ members are indicated by triangles and squares, respectively.

If we lower/increase the optimal value $\mathcal{R}_{min} = 1 \text{ h}^{-1} \text{ Mpc}$ by 20% the cumulative and differential distribution functions are still consistent with being unbiased down to 200 km s^{-1} (the KS associated probability drops to $(40 \pm 33)\%/(50 \pm 30)\%$ respectively), but the overall number of reconstructed systems would also decrease/increase by nearly 20%, for a total of 462 ± 20 (700 ± 50) systems per square degree.

The overall performance of the method can also be seen in figure 15 where we plot the intrinsic and recovered velocity dispersions on a cluster-by-cluster basis. Here we can see that occasionally a large system is fragmented into multiple components, some with very few members and low velocity dispersions. In an opposite sense, interlopers tend to increase the estimated velocity dispersion of smaller systems. This bias, which mostly affects the percolation algorithms, acts to steepen the slope of the $\sigma - \sigma$ relation. However our algorithm, by locally defining the clustering parameters, is able to counteract this tendency and elastically perform over a wide range of velocity dispersions. While the characteristics of the systems reconstructed using the FoF method are known to be fairly sensitive to the scale length of the adopted linking parameters (Frederic 1995a,b, Giuricin *et al.* 2000), there is no preferred velocity or richness scale artificially introduced into the VDM reconstructed systems; as a consequence the system velocity dispersion can be efficiently used as a stable and unbiased parameter to define a complete cluster sample (see §6).

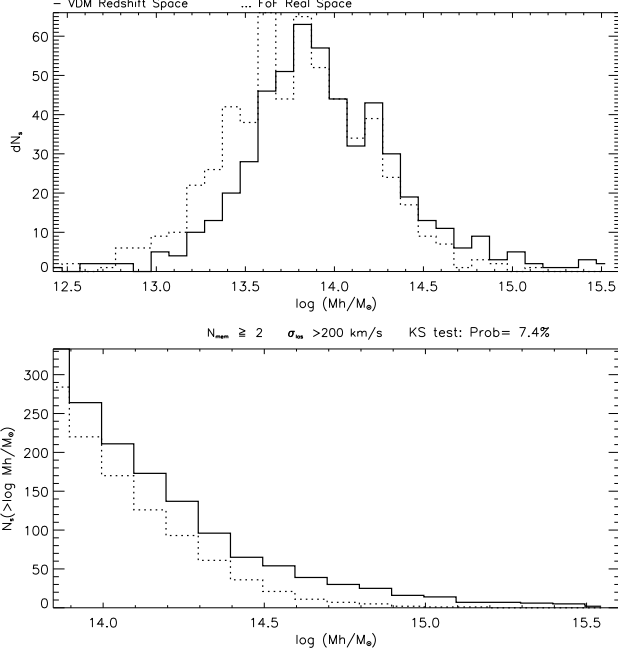


FIG. 16.— Differential (*upper*) and cumulative (*lower*) distributions of the number of clusters detected and reconstructed in mock catalog #1 as a function of their virial mass. The mass is computed using to the median mass estimator of Heisler, Tremaine & Bahcall (1985). The distribution of real-space groups is shown by the dotted line, while the observed distribution recovered in redshift space is the solid line. Data are binned in logarithmic mass intervals of width 0.1.

We next compute the virial mass of a system recovered in redshift space by the VDM and compare with the intrinsic value (see Appendix A). We are not concerned here with any biasing scheme that may relate the mass inferred from optical tracers to the true halo mass; we only investigate to what extent the virial analysis applied in the presence of a distance degeneracy along the line of sight is able to reproduce the virial mass estimate from the members of the same group identified in real space that are above the DEEP2 flux limit.

The hypotheses and approximations at the heart of the virial analysis are known to oversimplify reality (Bahcall & Tremaine 1981). Moreover the virial mass critically depends on the estimated cluster harmonic radius (see Appendix A), and it is easy to show that potential interlopers are the dominant source of systematic errors. While the galaxy distribution inside a cluster is described by a radially decreasing function (generally assumed to be a r^{-2} profile) the probability of interlopers increases as r^2 , leading to a systematic tendency to overestimate the harmonic radius of the recovered cluster. Even with a quadratic dependence on a reliable estimator such as the velocity dispersion, the mass estimate will be linearly affected by this systematic offset. This effect can be appreciated in figure 16 where we plot the differential and cumulative mass distributions for one of our mock simulations.

Even when the mass is evaluated only for in the regime where the velocity function is recovered accurately ($\sigma_{los} \gtrsim 200 \text{ km s}^{-1}$), we observe a systematic offset between the real- and redshift-space samples.

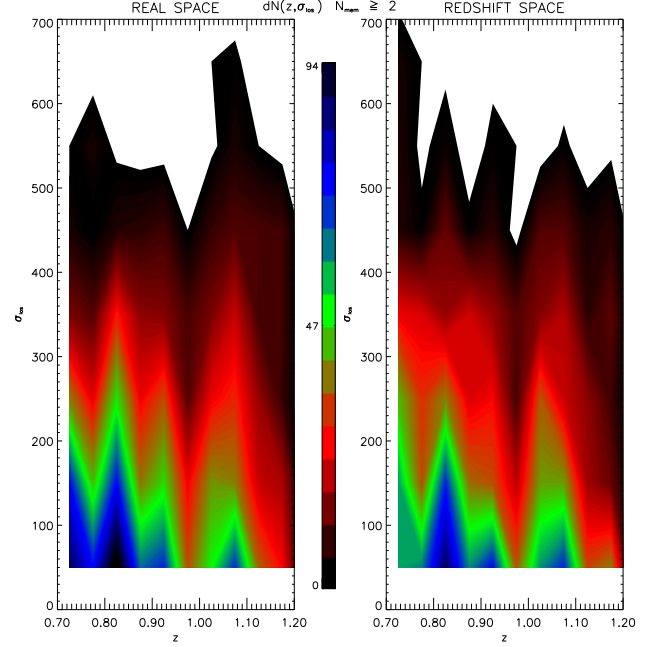


FIG. 17.— Differential number counts of clusters as a bivariate function of their redshift z and projected velocity dispersion σ_{los} . The parent distribution of cluster counts identified in real space is shown in the left panel, while the observed distribution recovered in redshift space with our method is plotted in the right panel. Density levels, smoothed by 0.05 in z and 50 km s^{-1} in σ_{los} , are represented by means of the colorbar.

This effect is only marginally corrected for by applying more robust methods such as the median mass estimator of Heisler, Tremaine & Bahcall (1985) (see eq. 12 in that work). A better agreement between real and reconstructed mass distributions may be achieved by lowering \mathcal{R}_{min} by 10% from its nominal value ($1 h^{-1} \text{ Mpc}$). In this way a satisfactory degree of agreement is reached for systems with $M \geq 10^{14} h^{-1} M_{\odot}$. In analyzing all the six mock catalogs we then reconstruct an average of 160 ± 22 groups per square degree out of the original 193 ± 8 real systems with accurate mass statistics.

In a previous paper (Newman et al. 2001) we showed that the evolution of the comoving abundance of clusters as a function of their velocity dispersion σ and redshift z is a sensitive function of cosmological parameters. The statistical significance and robustness of the cluster abundance test depends critically on an unbiased mapping of the distributions of the cluster observables from real to redshift space. How well this can be achieved is seen in figure 17 where we show that the reconstructed statistic is a satisfactorily undistorted reproduction of the underlying real $N(\sigma, z)$ function. The large number of recovered systems, together with the small fluctuations in the total number of clusters observed in the six independent mock catalogs (reflected by their small variance, $\sim 7\%$ of the mean value) should allow us to perform the test without systematic biases. It is necessary only to tune \mathcal{R}_{min} with a reasonable set of simulations to ensure that both the total number of clusters and their distribution will be reconstructed successfully over some range in velocity dispersion.

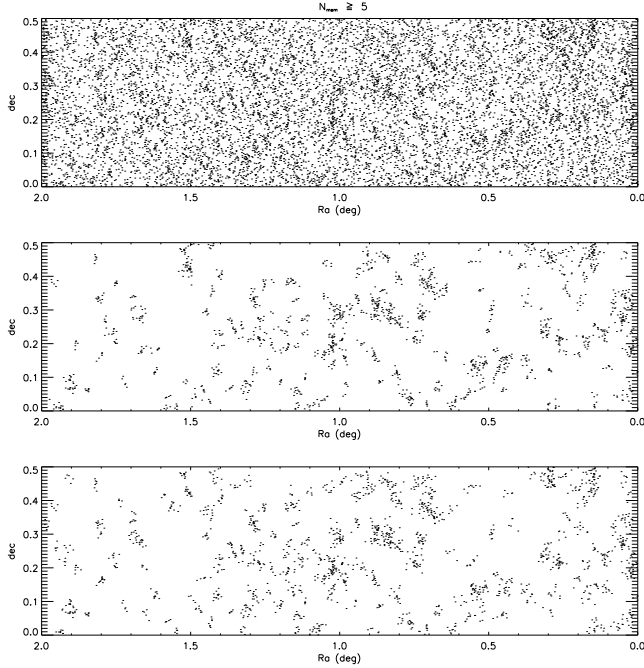


FIG. 18.— *Upper*: sky distribution of DEEP2 target galaxies selected to be on a slitmask for mock catalog #1, also represented in fig 11. *Center*: sky distribution of mock catalog #1 selected galaxies belonging to real-space groups with more than 5 elements assigned to DEEP2 masks. *Lower*: sky distribution of galaxies associated to groups with more than 5 elements by our VDM algorithm applied to mock catalog #1 selected targets only.

5. EFFECTS OF DEEP2 TARGET SELECTION BIAS

In the four DEEP2 fields, individual slitmasks will each cover overlapping $16'$ by $4'$ regions. There will be ~ 130 slitlets per mask, but the mean surface density of candidate galaxies still exceeds the number of objects we can select, and spectra of selected targets cannot be allowed to overlap on the CCD. Spectra will thus be obtained for $\sim 70\%$ of the galaxies in each field that meet our color and magnitude selection criteria, with the specific objects chosen by a slitmask algorithm which is necessarily biased against the highest-density regions, where the spectra of neighboring galaxies would overlap on the CCD. Here we test how this bias, which forces us to observe a lower fraction of targets in the densest regions (like the cores of clusters) will affect VDM results. We can use the same sample to investigate to what velocity dispersion the sample of clusters recovered from DEEP2 will be complete.

Figure 18 shows the results of our target selection on mock galaxy catalog #1. The upper panel shows the sky distribution of galaxies which would be targeted to be on a slitmask (mock #1 targets). A comparison of this galaxy map with the upper panel of figure 11, which shows all the galaxies in that field, shows the effects of our target selection strategy which is necessarily most strongly biased on small projected scales. Note the smoother spatial density contrast compared to the clumpy distribution in figure 11.

The specific DEEP2 observing strategy can be easily incorporated when applying the VDM; we simply increase the value of \mathcal{R}_{\min} by a factor $s^{-1/3}$, where s is the fraction of all target objects that are selected for observation.

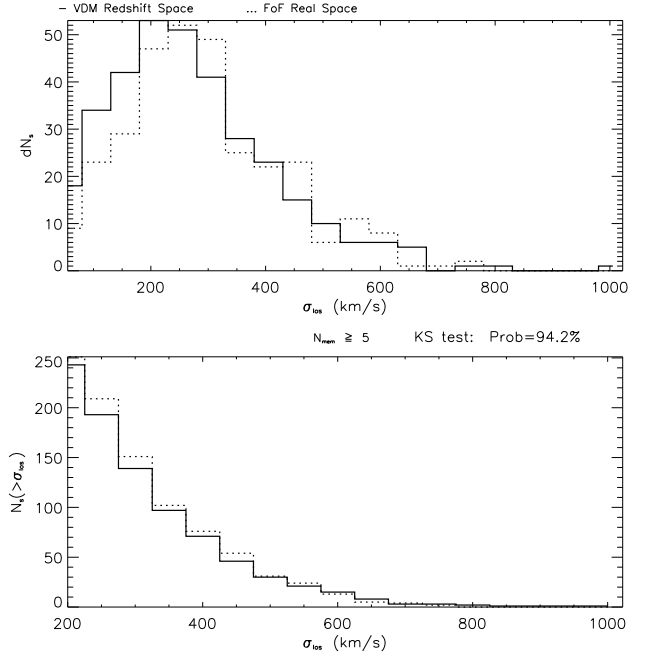


FIG. 19.— Differential (*upper*) and cumulative (*lower*) distributions of the number of clusters with $N_{\text{mem}} \geq 5$ elements found in mock catalog #1 as a function of their projected velocity dispersions. The distribution of velocity dispersions derived from all galaxies meeting the DEEP2 magnitude limit in each system in the real-space mock catalog is shown by the dotted line, while the observed distribution recovered by VDM in redshift space after applying the DEEP2 slitmask target selection criteria is plotted as a solid line. Data are binned in velocity dispersion intervals of width 50 km s^{-1} . A Kolmogorov-Smirnov test confirms the consistency.

This counteracts the fact that our sampling of necessity dilutes the central regions of clusters and thus could bias the algorithms in the detection phase (§3.2.1). In the central panel of figure 18 we plot the map of galaxies assigned slitlets by our selection procedure and which belong to real-space groups with at least 5 members selected for observation, while in the lower panel we plot the galaxies belonging to groups ($N_{\text{mem}} \geq 5$) identified by applying the VDM to the redshift-space catalog of selected targets in mock catalog #1. These plots graphically show that the map of targeted cluster members detected by the algorithm traces the same structure as the map of galaxies which are known to be members of real clusters in the targeted sample.

We next investigate how the DEEP2 target selection biases affect the σ_{los} threshold above which cluster members are reliably identified and reconstructed by the VDM. In figure 19 we plot the distribution of the number of clusters as a function of their line of sight velocity dispersion. Both the real distribution (derived including all galaxies meeting the DEEP2 magnitude limit, not just those assigned slitlets) and the distribution recovered by the VDM after applying to the sample our slitmask design algorithm (mock catalog #1 targets) are shown. The threshold of unbiased identification, $\sigma_{\text{los}} \approx 200 \text{ km s}^{-1}$, is now reached only if we implement a second selection parameter which discriminates groups according to their richness.

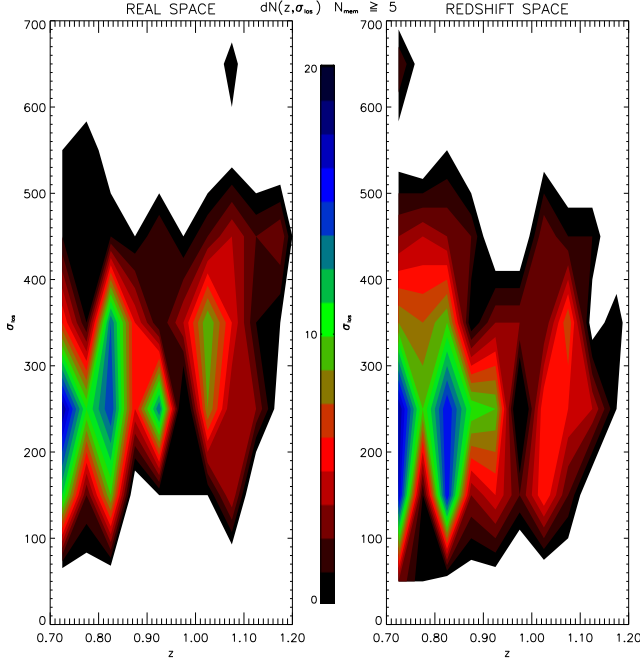


FIG. 20.— Differential number counts of clusters as a simultaneous function of their redshift z and projected velocity dispersion σ_{los} for systems with $N_{mem} \geq 5$ members. The parent distribution of cluster counts identified in real space is shown on the left, while the observed distribution recovered by VDM in redshift space after applying to the galaxy sample the DEEP2 target selection criteria is plotted on the right. Density levels, smoothed by 0.05 in z and 50 km/s in σ_{los} , are represented by means of the colorbar.

An acceptable fit between real and reconstructed distributions (average KS probability of $(35 \pm 30)\%$ for the six mocks) is obtained if we require $N_{mem} \geq 5$. The average number of real clusters with $N_{mem} \geq 5$ and $\sigma \geq 200$ km s $^{-1}$ in the six mocks is 268 ± 16 per square degree, while the average number of systems with the same characteristics reconstructed in redshift space after applying the DEEP2 target selection algorithm to the mocks is 271 ± 13 . By lowering/increasing the initial \mathcal{R}_{min} parameter by 20% we would have recovered 205 ± 14 / 340 ± 11 systems per square degree with an average KS probability of $(20 \pm 24)\%$ / $(30 \pm 34)\%$.

If we do not place conditions on richness, then the reconstructed sample matches the real cluster distribution for $\sigma_{los} \gtrsim 400$ km s $^{-1}$ (average KS probability $(30 \pm 20)\%$). The average number of systems meeting this condition in our six mocks is 135 ± 11 per square degree while the reconstructed number is 109 ± 11 . This selection would degrade the sample statistics by a factor of ~ 2 . The actual target selection used in the DEEP2 survey will incorporate adaptive tiling of the slitmasks; this has not been included in the discussion here and it should somewhat reduce selection biases.

We have shown that the VDM algorithm works efficiently without applying any predetermined selection correction as a function of redshift. This can be seen in figure 20 where we plot the simultaneous distribution of clusters as a function of both line of sight velocity dispersion and redshift. Median values for global parameters (see appendix A for their definition) characterizing real and

reconstructed groups are listed in table A1 for two specific samples (mock catalog #1 and mock catalog #3). We note the typical offset that characterizes quantities whose definition requires computation of the system radius. It is also interesting to note that a quantity seriously biased by the DEEP2 mask design criteria is the system mass-to-light ratio. This is a joint conspiracy of the bias in the calculated mass and of the fact that the total luminosity of a system is severely underestimated when only targets selected for DEEP2 observation are considered.

6. COMPLETENESS WITH RESPECT TO THE MATTER DISTRIBUTION

From a theoretical perspective it is easier to predict how mass evolves into structures than to describe how it is converted into light (Kochanek 2001). Observationally, however, catalogs of groups and clusters of galaxies represent only visible tracers of the general underlying matter fluctuations. If we want to use the abundance of galaxy clusters to put constraints on cosmological quantities as suggested by many authors (Fan, Bahcall, & Cen 1997; Pen 1998; Henry 2000; Borgani et al. 2001; Moscardini, Matarrese, & Mo 2001; Newman et al. 2001) it is therefore imperative to assess the completeness of the reconstructed group sample with respect to the underlying parent distribution of matter halos (White & Kochanek 2001).

In section 4 we argued that the distribution of clusters as a function of their line of sight velocity dispersion can be reliably determined using our VDM algorithm down to $\sigma_{los} \gtrsim 200$ km s $^{-1}$. We here investigate to what extent the $N(\sigma_{los})$ distribution inferred using a flux-limited sample of galaxies as a tracer of the clusters reproduces the statistics of dark matter fluctuations. The region of velocity space where the agreement is satisfactory determines the range of completeness of our cluster sample and the region of feasibility of cosmological tests based upon it.

Since the VDM algorithm is based upon the use of locally determined parameters, it is highly independent of the particular cosmological simulation used to test it. However we expect that the halo occupation number, i.e. the rate at which galaxies form in a halo as a function of mass, will vary in different cosmological scenarios (Peacock & Smith 2000; Marinoni & Hudson 2001); as a consequence the interval of consistency between halo and cluster velocity dispersions can be a function of the assumed cosmological model. We therefore frame the conclusions of this section within the standard picture of the Λ CDM model described in §2. Moreover, due to the uncertainties affecting prescriptions for galaxy formation, conclusions we draw in this section may be sensitive to simulation details.

In figure 21 we show the distribution of systems in mock catalog #1 as a function of the line-of-sight velocity dispersion parameter inferred from *all* the galaxies in the halo, applying no magnitude limit. We may expect that these galaxies should be less biased compared to the dark matter than the $\sim L_*$ galaxies that DEEP2 will observe, and thus should approximate the velocity dispersion of the mass in each cluster. Superimposed, we also plot the distribution of clusters recovered by VDM in redshift space inferred from the galaxies brighter than the DEEP2 magnitude limit. Note that in both cases we derive the velocity dispersion using the

same computational scheme; only the tracers are different.

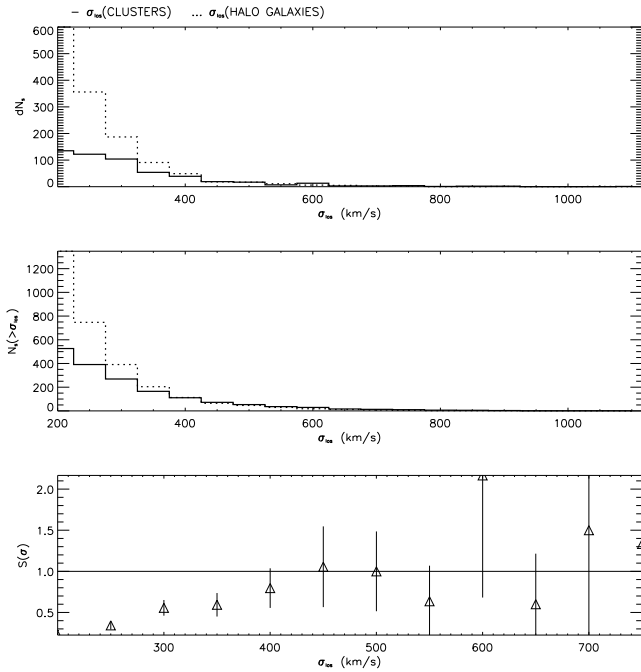


FIG. 21.— The solid lines show the differential (*upper*) and cumulative (*center*) σ_{los} distributions of VDM clusters in mock catalog #1 (solid line) is plotted as a function of the projected velocity dispersion. Also plotted are the σ_{los} distributions of halos identified in real space with a velocity dispersion inferred using all the galaxies that form within the halo, not just those meeting the DEEP2 magnitude limit (dotted line). Data are binned in velocity dispersion intervals of width 50 km s^{-1} . *Lower*: The sample selection function in velocity dispersion space. In this Λ CDM simulation, clusters recovered by VDM in redshift space are representative of the general halo population for $\sigma_{los} \gtrsim 400 \text{ km s}^{-1}$.

We also define a velocity dispersion selection function as the fraction of the clusters identified in redshift space with velocity dispersion σ_{los} out of the total number of matter halos having that same velocity dispersion. It is clear from figure 21 that the lower threshold of completeness is $\sim 400 \text{ km s}^{-1}$ below which the selection function significantly departs from unity. Above this limit, the velocity dispersion inferred from the most luminous galaxies identified as cluster members by our method is consistent with the parent σ distribution of halos, i.e. the effects of any possible luminosity-dependent velocity bias are minimal. Note that to the same velocity limit, the VDM sample is also not affected by the DEEP2 mask design biases. It may be possible to use the derived selection function to correct for unseen halos much in the same way we correct for unseen galaxies when we compute the galaxy luminosity function in a flux-limited survey.

The mass distribution of halos can be economically described in terms of analytical formulas (Press & Schechter 1974; Sheth & Tormen 1999). A similar halo description in terms of velocity dispersions can be derived assuming a conversion prescription between the mass M and the one dimensional velocity σ_{halo} (Narayan & White 1988; Kochanek 1995; Newman et al. 2001). However, the velocity dispersion of a halo can be computed according to at least two different operative definitions.

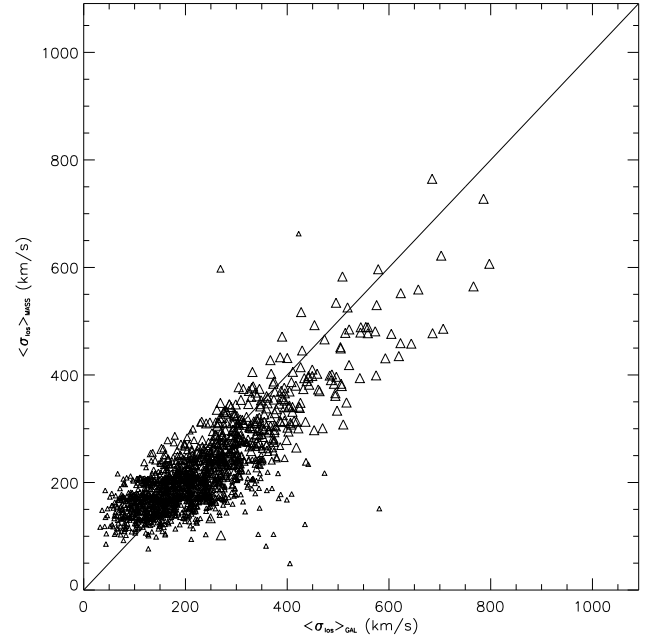


FIG. 22.— Correlation between two estimators of the velocity dispersions of systems simulated in a Λ CDM model (for mock catalog #1; see §2). Along the x-axis we plot the line of sight velocity dispersion of the halos inferred applying the estimator described in appendix A (eq. A3) to all the galaxies that form in the halo (σ_{gal}). The velocity dispersion inferred using a spherical isothermal model to describe the halo mass distribution, σ_{mass} , is plotted along the ordinate axis. The triangles are scaled accordingly to the following three halo richness ranges: $10 \leq N_{gal} \leq 10$, $10 < N_{gal} \leq 20$, and $N_{gal} > 20$. The panel shows that the different σ estimates are correlated but offset (the solid line is the curve $\sigma_{gal} = \sigma_{mass}$).

We can estimate σ_{los} by applying the standard estimator given in Appendix A (eqn. A3) to all the galaxies that form within a halo. Alternatively, in the spherical top-hat collapse model, a halo's mass may be defined in terms of r_{200} , the radius of a spherical volume within which the mean density is 200 times the critical density at that redshift, and given by

$$M_{200} = \frac{4\pi}{3} <\rho(r)>_{r_{200}} r_{200}^3.$$

In the case of a singular isothermal spherical particle distribution, the density is related to the velocity dispersion (Binney & Tremaine 1987) as

$$\rho(r) = \frac{\sigma_{los}^2}{2\pi G r^2};$$

therefore the one-dimensional velocity dispersion of each halo can be derived as a function of M_{200} and r_{200} .

In comparing the results of simulations such as those used for this paper to semi-analytic predictions, it is important to understand the relationship between what is measured observationally (using techniques such as that of eqn. A3) with what is predicted (which is closer to the methods of eqns. 3 & 4). We thus have compared the results of applying a velocity dispersion estimator based on spherical averages (implicitly assuming a spherical isothermal model) to the line-of-sight velocity dispersion σ_{gal} obtained by applying the point estimator given

in appendix A (eq. A3), applying each to the real-space FoF catalog of systems (our standard comparison sample).

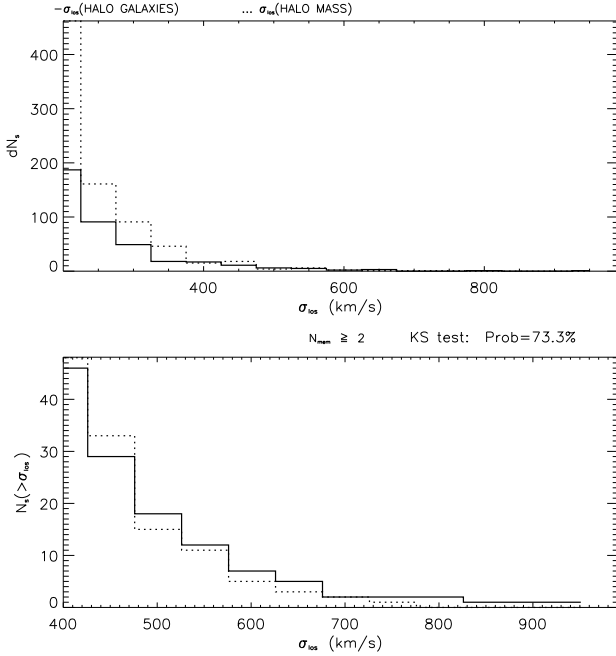


FIG. 23.— Differential (*upper*) and cumulative (*lower*) velocity dispersion distributions of systems identified via FoF in real space for mock catalog #1 and using two different methods of calculation: applying the estimator described in appendix A (eq. A3) to all the galaxies that form in the halo (solid line) and using a spherical isothermal model to describe the halo mass distribution (dotted line). Data are binned in velocity dispersion intervals of width 50 km s^{-1} . Due to the offset between the two indicators (see Fig. 22), we have re-mapped σ_{los} inferred using galaxies by shifting each estimated value lower by 50 km s^{-1} . A Kolmogorov-Smirnov test confirms the consistency.

In figure 22 we show the scatter diagram between the two estimators applied to halos that harbor at least 2 galaxies (regardless of their luminosity). Compared to figure 21, the scatter in figure 22 is substantial, since the groups found by FoF can be quite irregularly shaped. In addition to that scatter, systematic deviations from equality are apparent; in the low velocity regime ($\sigma_{gal} \leq 300 \text{ km s}^{-1}$) we have $\sigma_{halo} > \sigma_{gal}$ systematically, while for more massive systems the spherical estimator is biased low with respect to σ_{gal} . Although the galaxy-based velocity estimator may be less reliable in the small-system limit and the reality of that deviation less certain, there is a known tendency for larger groups to be more irregularly shaped, since FoF generally links galaxies well outside r_{200} . This in turn causes the two operational definitions of velocity dispersion to be biased in the same sense White (2001) found, using a different spherical model to describe the halo mass distribution.

These halo substructures are either real features or a problem caused by the spurious tendency of the FoF algorithm to merge close, pre-merging units. We can better understand the nature of this offset and the influence of substructure on the internal cluster dynamics by analyzing figure 23. Here we plot the number distribution of halos as a function of their differently estimated velocity

dispersions. After shifting each σ_{gal} estimate lower by 50 km s^{-1} , we note that the shape of the two distributions is approximately the same, as is confirmed by the relatively high value of the Kolmogorov-Smirnov probability parameter. This simple re-mapping strategy guarantees that at least in principle we can easily correct for the velocity definition being used in modeling the distribution of virialized systems as a function of their velocity dispersions.

7. CONCLUSIONS

The Voronoi diagram and its dual, the Delaunay triangulation, are among the most useful data structures in computational geometry. The emphasis of this paper is to show how a three-dimensional implementation of these fundamental graphs, which provide an explicit representation of the relationships between neighboring points, can help in both identifying and reconstructing a complete sample of galaxy systems in a deep flux-limited redshift survey, with the sample selection function directly defined in terms of the velocity dispersion parameter. Our VDM algorithm uses locally specified clustering parameters, physically determined on a cluster by cluster basis, without requiring arbitrarily chosen global linking parameters. Since it is based on a neighboring relationship already encoded in the Delaunay complex, it is quite fast; only 5 minutes on a modern workstation processes ~ 15000 galaxies into a catalog of groups and clusters.

We have used a family of artificial catalogs simulating the spatial, velocity, and flux distributions of DEEP2 galaxies to study the performance of our method, to test its stability under variation of simple and physically justified clustering criteria, and to assess the level of completeness of the resulting catalog of systems.

From applying the method to six independent mock catalogs we conclude that:

i) The algorithm does not suffer from major distance-dependent effects and can be applied without any redshift-dependent correction to the parameters governing cluster reconstruction over the wide redshift baseline $z=0.7-1.2$ covered by the DEEP2 redshift survey. The resulting cluster catalog is fairly stable under variations as great as 20% of the selection parameters, and its members are identified in an unbiased way for groups with $\sigma_{los} \gtrsim 200 \text{ km s}^{-1}$ in a $I_{AB} \leq 23.5$ magnitude-limited survey.

ii) The recovered number density of systems as a bivariate function of velocity dispersion and redshift reproduces major features of the underlying real-space distribution. This function, essentially free from major statistical or systematic uncertainties, can be reliably used to constrain cosmological quantities as in Newman et al. (2001).

iii) The virial masses derived using samples of clusters complete in velocity dispersion match the actual cluster distribution poorly. Their values are biased high by the presence of interlopers which artificially increase the system radius.

iv) The necessity of avoiding overlapping spectra in the DEEP2 survey limits the sampling efficiency of spectroscopic target selection, especially in regions of the sky with higher than average surface density of galaxies. Taking into account this target selection bias, we expect to identify and reconstruct a homogeneous sample of ~ 270 clusters per square degree with $N_{\text{mem}} \geq 5$ elements and

velocity dispersion $\sigma_{\text{los}} \gtrsim 200 \text{ km s}^{-1}$ for a ΛCDM cosmology. Relaxing the richness condition, i.e. only requiring $N_{\text{mem}} \geq 2$, the unbiased sample would be a factor of 2 smaller, extending to $\sigma_{\text{los}} \sim 400 \text{ km s}^{-1}$.

v) Finally, comparing the distribution properties of VDM reconstructed galaxy systems and similar statistics of matter halos within a ΛCDM framework, we conclude that the recovered cluster sample is complete down to groups with $\sigma_{\text{los}} \gtrsim 400 \text{ km s}^{-1}$. This limit sets the lower threshold for meaningful comparisons with theoretical models of structure formation.

The DEEP2 survey is designed to be a comprehensive study of the Universe at $z = 1$. Having a sample of high redshift galaxies comparable in quality to those available locally will enable many independent tests of the evolution

of structure in the Universe. In this study we demonstrate that we expect DEEP2 to provide us not only with a complete database of galaxy positions and spectra, but also with a large, robust and complete catalog of deep, optically selected galaxy systems.

We would like to thank Guinevere Kauffmann for allowing us to use her semi-analytic GIF simulations. A special thanks also to Martin White and Chris Kochanek for enlightening discussions. We also acknowledge useful conversations with S. Borgani, J. di Francesco, and E. Scannapieco. This work is supported by National Science Foundation Grant No. AST-0071048 and by equipment donated by Sun Microsystems.

APPENDIX

DEFINITIONS OF SYSTEM PROPERTIES

The expression relating cosmological (z) and observed (z_o) redshifts is, in first order approximation, (Harrison 1974)

$$z = z_0 + \frac{v_p}{c}(1 + z_0) \quad (\text{A1})$$

where v_p (km s^{-1}) is the peculiar velocity along the line of sight. In the analysis of the ΛCDM mock catalogs, the relations between z_0 and r is determined using the comoving distance formula

$$r = \frac{c}{H_0} \int_0^z \frac{dz}{[\Omega_{0,m}(1+z)^3 + \Omega_\Lambda - \Omega_k(1+z)^2]^{1/2}}. \quad (\text{A2})$$

The *line of sight velocity dispersion* in a group with N_{mem} members each at redshift z_i , corrected for relativistic effects (Harrison 1974), is

$$\sigma_{\text{los}} = \frac{1}{1 + \langle z \rangle} \sqrt{\frac{\sum_{i=1}^{N_{\text{mem}}} (cz_i - \langle cz \rangle)^2}{(N_{\text{mem}} - 1)}}. \quad (\text{A3})$$

A formal estimate of the standard error in σ_{los} is then given by (Bevington 1969):

$$\sigma(\sigma_{\text{los}}) = \frac{1}{2} \sigma_{\text{los}} \sqrt{\frac{2}{N_{\text{mem}}} \left(1 - \frac{1}{N_{\text{mem}}}\right)}. \quad (\text{A4})$$

The *mean pairwise separation* in a group at distance z_{gr} may be calculated according to the approximate formula

$$R_p \equiv \langle |\mathbf{r}_{ij}| \rangle \approx \frac{4}{\pi} d_{\text{ang}}(z_{gr}) \langle \theta_{ij} \rangle, \quad (\text{A5})$$

where

$$\langle \theta_{ij} \rangle \equiv \frac{\sum_i \sum_{j>i} \theta_{ij}}{N_{\text{pair}}}, \quad (\text{A6})$$

N_{pair} is the number of distinct galaxy pairs in the group ($N_{\text{mem}}(N_{\text{mem}} - 1)/2$), $d_{\text{ang}}(z_{gr})$ is the comoving angular distance of the group at the given redshift, and θ_{ij} is the angular separation between group members i and j . Tucker et al. (2000) estimate the rms error in R_p to be

$$\sigma_{R_p} = \frac{R_p}{\langle \theta_{ij} \rangle} \sqrt{\frac{N_{\text{pair}} \sum_i \sum_{j>i} (\theta_{ij})^2 - \left(\sum_i \sum_{j>i} \theta_{ij}\right)^2}{(N_{\text{pair}} - 1) N_{\text{pair}}^2}}. \quad (\text{A7})$$

The group *harmonic radius* is approximately given by the formula

$$R_h \equiv \langle |\mathbf{r}_{ij}|^{-1} \rangle^{-1} \approx \frac{\pi}{2} \frac{d_{\text{ang}}(z_{gr})}{\langle \theta_{ij}^{-1} \rangle}, \quad (\text{A8})$$

while its error will be

$$\sigma_{R_h} = \frac{R_h}{\langle \theta_{ij}^{-1} \rangle} \sqrt{\frac{N_{\text{pair}} \sum_i \sum_{j>i} (\theta_{ij}^{-1})^2 - \left(\sum_i \sum_{j>i} \theta_{ij}^{-1}\right)^2}{(N_{\text{pair}} - 1) N_{\text{pair}}^2}}. \quad (\text{A9})$$

The *crossing time* for a group, in Hubble time units, is defined as in Nolthenius & White (1987):

$$\frac{t_{cr}}{t_H} = \frac{2R_h}{\sqrt{3}\sigma_{los}} \left[1 \pm \sqrt{\frac{\sigma_{R_h}^2}{R_h^2} + \frac{\sigma_{los}^2}{\sigma_{los}^2}} \right]. \quad (A10)$$

Comparing this time to the time needed for a homogeneous sphere to collapse out of the Hubble flow, we can formally conclude that a system is virialized if $t_{cr} < 0.34 t_H$.

The group's virial mass is estimated to be

$$M_{vir} = \frac{6\sigma_{los}^2 R_h}{G} \left[1 \pm \sqrt{\frac{4\sigma_{los}^2}{\sigma_{los}^2} + \frac{\sigma_{R_h}^2}{R_h^2}} \right], \quad (A11)$$

where G is the gravitational constant.

A more stable mass estimator, less sensitive to interlopers, is the median mass defined as (Heisler, Tremaine & Bahcall 1985).

$$M_{med} = \frac{f}{G} d_{ang}(z_{gr}) Med_{ij}[(v_i - v_j)^2 \theta_{ij}], \quad (A12)$$

where v is the velocity of the cluster members with respect to the cluster centroid, corrected for relativistic effects, and where f is a dimensionless fudge factor determined from numerical experiments and whose value is set to 6.5.

We reconstruct the total luminosity of each system using the weighting scheme of Marinoni, Hudson & Giuricin (2001), i.e. we write the total expected luminosity of the system as

$$L_s(r) = L_{obs}(r) + \tilde{L}(r) = L_{obs}(r)w_L(r), \quad (A13)$$

where \tilde{L} denotes the unseen luminosity from galaxies below the magnitude limit and $w_L(r)$ is the *luminosity-density weighting function*

$$w_L = \frac{\int_0^\infty L\phi(L)dL}{\int_{L_{lim}(d)}^\infty L\phi(L)dL}. \quad (A14)$$

A formal estimate of the rms error is obtaining by summing in quadrature the errors of the single luminosities L_i of the group members as follows:

$$\sigma_{L_s} = w_L N_{mem} \sqrt{\frac{\langle L_i^2 \rangle - \langle L_i \rangle^2}{N_{mem} - 1}}. \quad (A15)$$

REFERENCES

- Abell, G. O. 1958, ApJS, 3, 211
 Ahuja, N. 1982, IEEE Transaction on Pattern Analysis & Machine Intelligence, 4, 336
 Ahuja, N., & Tuceryan, M. 1988, Computer Vision Graphics and Image Processing, 48, 304
 Aurenhammer, F. 1991, ACM Computing Surveys, 23, 345
 Bahcall, N. A. 1981, ApJ, 247, 787
 Bahcall, N. A. 1989, ARA&A, 26, 631
 Bahcall, N. A., Fan, X., & Cen, R. 1997, ApJ, 485, L53
 Bahcall, J. N., & Tremaine, S. 1981, ApJ, 244, 805
 Barber, C. B., Dobkin, D. P., & Huhdanpaa, H. T. 1996, *ACM Transaction on Mathematical Software*, 22, 469
 Benson, A. J., Cole, S., Frenk, C. S., Baugh, C. M., & Lacey, C. G. 2000, /mnras, 311, 793
 Bevington, P. R. 1969, *Data reduction and error analysis for the physical science*, McGraw-Hill, New York
 Binney, J., & Tremaine, S. 1987, *Galactic Dynamics* (Princeton: Princeton Univ. Press), 228
 Biviano, A., Mazure, A., Adami, C., Katgert, P., den Hartog, R., de Theije, P., & Rhee, G. 1998, in ASP Conf. Ser. 176, *Observational Cosmology: The Development of Galaxy Systems*, ed. G. Giuricin, M. Mezzetti, & P. Salucci, (San Francisco:ASP), 15
 Borgani, S., Gardini, A., Girardi, M., & Gottloeber, S. 1997, *New Astronomy*, 2, 119
 Borgani, S., Rosati, P., Tozzi, P., Stanford, S. A., Eisenhardt, P. R., Lidman, C., Holden, B., Della Ceca, R., Norman, C., & Squires, G. 2001, ApJ, 561, 13
 Cole, S., & Lacey, C. G. 1996, MNRAS, 281, 716
 Coles, P. 1991, *Nature*, 349, 288
 Cowley, D. J., Faber, S., Hilyard, D. F., James, E., & Osborne, J. 1997, SPIE, 2871, 1107
 Davis, M., Newman, J. A., Faber, S. M., & Phillips, A. C. 2000, *Proceedings of the ESO/ECF/STSCI Workshop on Deep Fields*, Garching Oct 2000, (Publ: Springer)
 Delaunay, B. 1934, Bull. Acad. Sci. USSR(VII) p. 793
 Descartes, R. 1644, *Le Monde, ou Traite de la Lumiere*, Abaris Books, New York
 Dirichlet, G., L. 1850, J. Reine Angew. Math., 40, 209
 Ebeling, H., & Wiedenmann, G. 1993, sical Review E, 47, 704
 Estivill-Castro V., & Lee, I. 2000, in *Proceedings of the 5th International Conference on Geocomputation*
 Fadda, D., Slezak, E., & Bijaoui, A. 1997, Astr. Astrophys. Suppl. 127, 335
 Fan, X., Bahcall, N. A., & Cen, R. 1997, ApJ, 490, L123
 Frederic, J. J., 1995a, ApJS, 97, 259
 Frederic, J. J., 1995b, ApJS, 97, 275
 Frenk, C.S., White, S. D. M., Efstathiou, C., & Davis M. 1990, ApJ, 351, 10
 Gal, R. R., de Carvalho, R. R., Odewahn, S. C., Djorgovski, S. G., & Margoniner, V. E. 2000, AJ, 119, 12
 Garcia, A. M. 1993, Astr. Astrophys. Suppl. 100, 47.
 Giuricin, G., Marinoni, C., Ceriani, L., & Pisani, A. 2000, ApJ, 543, 178
 Giuricin, G., Samurović, S., Girardi, M., Mezzetti, M., & Marinoni, C. 2001, ApJ, 554, 857
 Gladders, M. D., & Yee, H. K. C. 2000, AJ, 120, 2148
 Gonzalez, A. H., Zaritsky, D., Dalcanton, J. J., & Nelson, A. 2001, ApJS, 137, 117
 Gourgoulhon, E., Chamaraux, P. & Fouqué, P. 1992, A&A, 255, 69
 Groth, E. J., Kristian, J. A., Lynds, R., O'Neil, E. J., Balsano, R., Rhodes, J., & the WFPC-1 IDT. 1994, BAAAS, 185, 5309
 Harrison, E. R. 1974, ApJ, 191, L51
 Haynes, M. P., & Giovanelli, R. 1991, AJ, 102, 841
 Heisler, J., Tremaine, S., & Bahcall, J. N. 1985, ApJ, 298, 8
 Henry, P. J. 2000, ApJ, 534, 565
 Huchra, J. P. & Geller, M. 1982, ApJ, 257, 423
 Icke, V., & van der Wegaert, R. 1987, A&A, 184, 16
 Icke, V., & van der Wegaert, R. 1991, A&A, 184, 16

- Ikeuchi, S. & Turner, E. L. 1991, MNRAS 250, 519
- Jain, A. K., & Dubes, R. C. 1988, *Algorithms for Clustering of Data*, Prentice Hall, New Jersey
- Jenkins, A., Frenk, C. S., White, S. D. M., et al. 2000, MNRAS, 321, 372
- Kang, I., Kim, T., & Li, K., 1997, in *Proceedings of the 5th International Workshop on Advances in Geographic Information Systems* (GIS-97), 35
- Kauffmann, G., Colberg, J. M., Diaferio, A., White, S. D. M. 1999, MNRAS, 303, 188
- Kim, R.S.J., et al. 2001, AJ, in press, astro-ph/0110259
- Kochanek, C. S. 1995, ApJ, 453, 545
- Kochanek, C. S. 2001, in *The Dark Universe*, ed M. Livio, Cambridge University Press (astro-ph/0108160)
- Le Fèvre, O., Vettolani, G., Maccagni, D., et al. 2001, in Proc. of the ESO/ECF/STSCI "Deep Fields" workshop, Springer (astro-ph/0101034)
- Lilje, P.B. 1992, ApJ, 386, L33
- Ling, E. N. 1987, PhD thesis, University of Sussex
- Maia, M. A. G., da Costa, L. N. & Latham, D. W. 1989, ApJS, 69, 809
- Marinoni, C. 2001, PhD thesis, University of Trieste
- Marinoni, C., Hudson, M. J., & Giuricin, G. 2001, ApJ, submitted, astro-ph/0109132
- Marinoni, C., & Hudson, M. J. 2001, ApJ, submitted, astro-ph/0109134
- Materne, J. 1978, A&A, 63, 401
- Matsuda, T., & Shima, E. 1984, *Prog. theor. Phys.*, 71, 855
- Mazure, A., Katgert, P., den Hartog, R., et al. 1996, A&A, 310, 8
- Moscardini, L., Matarrese, S., & Mo, H. J. 2001, MNRAS, 327, 422
- B. Mirtich, 1996, Journal of Graphics Tools, volume 1, number 2
- Narayan, R., & White, S. D. M. 1988, MNRAS, 275, 720
- Newman, J. A., & Davis, M. 2000, ApJ, 534, 11
- Newman, J. A., Marinoni, C., Coil, A. L., & Davis, M. 2001, PASP, in press, astro-ph/0109131
- Nolthenius, R. 1993, ApJS, 85, 1
- Nolthenius, R., & White, S. D. M. 1987, MNRAS, 235, 505
- Okabe, A., Boots, B., & Sugihara, K. 1992, *Spatial tessellations: concepts and applications of Voronoi diagrams*, Wiley & Sons, New York
- Openshaw, S. 1984, in Spatial Analysis and GIS, 83, eds. Fotheringham, S., & Rogerson, P., Taylor and Francis, London
- Park, C., Vogele, M. S., Geller, M. J., & Huchra, J. P. 1994, ApJ, 431, 569
- Pasztor, L. 1994, ASP Conference Series, 61
- Peacock, J. A., & Smith, R. E., 2000, MNRAS, 318, 1144
- Pen, U.-L. 1998, ApJ, 498, 60
- Press, W. H., & Schechter, P. 1974, ApJ, 187, 425
- Ramella, M., Geller, M. J. & Huchra, J. P. 1989, ApJ, 344, 57
- Ramella, M., Pisani, A. & Geller, M. J. 1997, AJ, 113, 483
- Ramella, M. et al. 1999, A&A, 342, 1
- Ramella, M. et al. 2001, A&A, in press, (astro-ph/0101411)
- Scodeggio, M., Olsen, L. F., da Costa, L., Slijkhuis, R., Benoist, C., Deul, E., Erben, T., Hook, R., Nonino, M., Wicenec, A., & Zaggia, S. 1999, Astr. Astrophys. Suppl. 137, 83
- Sheth, R. K., & Tormen, G. 1999, MNRAS, 308, 119
- Trasarti-Battistoni, R. 1998, Astr. Astrophys. Suppl. 130, 341
- Tucker, D. L., Oemler, A., Hashimoto, Y., Shectman, S. A., Kirshner, Robert, P., Lin, H., Landy, S. D., Schechter, P. L., & Allam, S. S. 2000, ApJS, 130, 237
- Tully, R. B. 1980, ApJ, 237, 390
- Tully, R. B. 1987, ApJ, 321, 280
- van der Wegaert, R. 1994, A&A, 283, 361
- van der Wegaert, R., & Icke, V. 1989, A&A, 213, 1
- Voronoi, G., 1908, J. Reine Angew. Math. 134, 198
- Wegner, G., Haynes, M. P., & Giovanelli, R. 1993, AJ, 105, 1251
- Wilson, G., Kaiser, N., Luppino, G. A., & Cowie, L. L. 2000, preprint astro-ph/0008504
- White, M. 2001, A&A, 367, 27
- White, M., & Kochanek, C. S. 2001, astro-ph/0110307
- Yoshioka, S., & Ikeuchi, S. 1989, ApJ, 341, 16
- Zaninetti, L. 1990, A&A, 1990, A&A, 233, 293

TABLE A1
MEDIAN GROUP PROPERTIES IN REAL AND REDSHIFT SPACE MOCK CATALOGS

Catalog		Sample I ^a		Sample II ^b		Sample III ^c	
		r-space	z-space	r-space	z-space	r-space	z-space
Mock #1	N_s	1678	1517	571	528	251	243
	$\text{Med}(N_{\text{mem}})$	2	4	4	6	7	7
	$\text{Med}(R_P)$	0.41	0.85	0.53	0.9	0.66	1.07
	$\text{Med}(R_H)$	0.42	0.71	0.48	0.68	0.54	0.80
	$\text{Med}(t_{\text{cr}})$ (Hubble time)	0.33	0.55	0.17	0.24	0.18	0.25
	$\text{Med}(\sigma_{\text{los}})$	136	133	301	302	328	327
	$\text{Med}(M_v)(10^{13}M_\odot)$	0.9	1.64	5.9	8.3	7.7	11
	$\text{Med}(M_v)(10^{13}M_\odot)$	1.2	1.9	6.9	8.8	7.4	11
	$\text{Med}(L_v)(10^{11}L_\odot)$	0.7	1.1	1.3	1.9	2.8	2.2
	$\text{Med}(M/L)(M_\odot/L_\odot)$	119	119	378	362	264	450
Mock #3	N_s	1822	1764	624	578	287	290
	$\text{Med}(N_{\text{mem}})$	2	4	4	6	8	7
	$\text{Med}(R_P)$	0.38	0.85	0.49	0.87	0.64	1.05
	$\text{Med}(R_H)$	0.38	0.69	0.44	0.66	0.49	0.81
	$\text{Med}(t_{\text{cr}})$ (Hubble time)	0.31	0.53	0.16	0.23	0.16	0.27
	$\text{Med}(\sigma_{\text{los}})$	135	130	297	305	335	317
	$\text{Med}(M_v)(10^{13}M_\odot)$	0.9	1.4	5.4	8.4	7.32	11.4
	$\text{Med}(M_v)(10^{13}M_\odot)$	1.1	1.6	6.6	9.5	7.37	10.6
	$\text{Med}(L_v)(10^{11}L_\odot)$	0.7	1.1	1.3	2.2	2.90	2.34
	$\text{Med}(M/L)(M_\odot/L_\odot)$	106	112	337	350	241	457

^aAll groups; i.e. systems with $N_{\text{mem}} \geq 2$ members

^bOnly groups with $\sigma_{\text{los}} \geq 200 \text{ km s}^{-1}$

^cOnly groups with $\sigma_{\text{los}} \geq 200 \text{ km s}^{-1}$ and $N_{\text{mem}} \geq 5$ extracted from the mock catalogs after applying the DEEP2 target selection criteria